










The significance of structural rich club hubs for the processing of hierarchical stimuli

Falko Mecklenbrauck^{1,2}  | Marius Gruber^{3,4}  | Sophie Siestrup^{1,2}  |
 Anoushiravan Zahedi^{1,2}  | Dominik Grotegerd³  | Marco Mauritz^{3,5}  |
 Ima Trempler^{1,2}  | Udo Dannlowski^{2,3}  | Ricarda I. Schubotz^{1,2} 

¹Department of Psychology, Biological Psychology, University of Münster, Münster, Germany

²Otto Creutzfeldt Center for Cognitive and Behavioral Neuroscience, University of Münster, Münster, Germany

³Institute for Translational Psychiatry, University of Münster, Münster, Germany

⁴Department for Psychiatry, Psychosomatic Medicine and Psychotherapy, University Hospital Frankfurt, Goethe University, Frankfurt, Germany

⁵Institute for Computational and Applied Mathematics, University of Münster, Münster, Germany

Correspondence

Falko Mecklenbrauck, Department of Psychology, Biological Psychology, University of Münster, Münster, Germany.
 Email: f_meck01@uni-muenster.de

Abstract

The brain's structural network follows a hierarchy that is described as rich club (RC) organization, with RC hubs forming the well-interconnected top of this hierarchy. In this study, we tested whether RC hubs are involved in the processing of hierarchically higher structures in stimulus sequences. Moreover, we explored the role of previously suggested cortical gradients along anterior-posterior and medial-lateral axes throughout the frontal cortex. To this end, we conducted a functional magnetic resonance imaging (fMRI) experiment and presented participants with blocks of digit sequences that were structured on different hierarchically nested levels. We additionally collected diffusion weighted imaging data of the same subjects to identify RC hubs. This classification then served as the basis for a region of interest analysis of the fMRI data. Moreover, we determined structural network centrality measures in areas that were found as activation clusters in the whole-brain fMRI analysis. Our findings support the previously found anterior and medial shift for processing hierarchically higher structures of stimuli. Additionally, we found that the processing of hierarchically higher structures of the stimulus structure engages RC hubs more than for lower levels. Areas involved in the functional processing of hierarchically higher structures were also more likely to be part of the structural RC and were furthermore more central to the structural network. In summary, our results highlight the potential role of the structural RC organization in shaping the cortical processing hierarchy.

KEYWORDS

cortical hierarchies, DWI, fMRI, nested hierarchies, rich club, structural connectivity

1 | INTRODUCTION

One of the most intriguing properties of the brain's connectome is the *rich club* (RC) phenomenon (van den Heuvel et al., 2012; van den Heuvel & Sporns, 2011). The RC consists of highly connected areas or

nodes, that is, *hubs*, which are also particularly well-connected with each other (Colizza et al., 2006), remarkably at the expense of high energetic costs (Collin, Sporns, et al., 2014; Harriger et al., 2012; van den Heuvel et al., 2012). Following its first discovery in the human connectome, the RC organization was consistently found as a

This is an open access article under the terms of the [Creative Commons Attribution-NonCommercial-NoDerivs](https://creativecommons.org/licenses/by-nc-nd/4.0/) License, which permits use and distribution in any medium, provided the original work is properly cited, the use is non-commercial and no modifications or adaptations are made.

© 2023 The Authors. *Human Brain Mapping* published by Wiley Periodicals LLC.

structural network property across different individuals and age groups (Ball et al., 2014; Grayson et al., 2014; Kocher et al., 2015; Riedel et al., 2022; Sporns, 2013). Van den Heuvel and Sporns (2013) theorized that the RC serves as a *global workspace* that integrates information from many different areas with unparalleled efficiency (Crossley et al., 2013; Harriger et al., 2012; Hermundstad et al., 2013; Zamora-López et al., 2010). However, since the RC organization as a graph theoretical property is foremost a mathematical construct (Griffa & van den Heuvel, 2018; Sporns, 2011), its functional role has yet to be clarified.

A strong argument in favor of the functional significance of the structural RC comes from clinical observations (for a review, see Griffa et al., 2013). Thus, changes in structural RC organization were found for autism and attention-deficit/hyperactivity disorder (Ray et al., 2014), Alzheimer's disease (R. Cao et al., 2020; Lee et al., 2018; Yan et al., 2018), bipolar disorder (Collin et al., 2017; O'Donoghue et al., 2017; Reavis et al., 2020; Wang, Deng, et al., 2019), and schizophrenia (Bassett et al., 2008; Collin et al., 2017; Collin, Kahn, et al., 2014; Reavis et al., 2020; van den Heuvel et al., 2013). Also, studies in nonclinical populations support a link between the structural RC organization and individual cognitive abilities (Baggio et al., 2015; Bathelt et al., 2018; Kim et al., 2016; Ma et al., 2017; Solé-Casals et al., 2019). Together, these observations point toward a very important function of the structural RC without specifying it in detail.

To understand the underlying function of the RC, Gollo et al. (2015) proposed that the RC organization enables the brain to produce slower and more stable dynamics in the rich and densely interconnected core while peripheral nodes of the network showed faster fluctuations. This multiscale temporal organization is crucial for the ability to process incoming stimuli by segregating or integrating hierarchically nested stimulus structures (Golesorkhi, Gomez-Pilar, Zilio, et al., 2021). These stimulus structures are omnipresent in our environment: Every action sequence toward a goal (Fitch & Martins, 2014; Grafton & Hamilton, 2007; Hamilton & Grafton, 1993; Wakita, 2014), every piece of music (Farbood et al., 2015) or paragraph of text (Lerner et al., 2011) requires hierarchical processing (for a review, see Jeon, 2014). A prominent hypothesis is that the brain's intrinsic hierarchical structure enables it to encode, decode, and process hierarchical structures in our environment (Botvinick, 2008; Hamilton & Grafton, 1993). Evidence in favor of this correspondence has been established by anatomical gradients in the frontal brain. Thus, a temporally organized processing gradient was suggested that follows an anterior-posterior axis (Badre & Nee, 2018; Chanes & Feldman Barrett, 2016; Dixon et al., 2017; Fuster, 2001; Hilgetag et al., 2016; Kiebel et al., 2008; Koehlin & Summerfield, 2007; Sanides, 1964), and a lateral to medial/midline gradient through the frontal cortex for the processing of hierarchically higher levels (W. H. Alexander & Brown, 2018; Badre & Nee, 2018).

Excitingly, it is unclear and remains to be investigated whether the RC architecture discussed above may underlie or correspond to these anatomical gradients. For instance, medial structures processing hierarchically higher structures in the stimulus (J. Chen et al., 2017; Hasson et al., 2015) were reliably demonstrated to be RC hub areas

(Q. Cao et al., 2013; Z. Chen et al., 2013; Huang et al., 2015; Riedel et al., 2022; Wang, Zhan, et al., 2019). However, the concept of a hierarchical processing gradient has not yet been empirically tested with relation to the RC architecture of the brain.

Against this background, in the present study we investigated whether the processing of hierarchically organized stimuli corresponds to the structural RC architecture and anatomical gradients of cortical processing hierarchies.

To this end, we collected diffusion weighted imaging (DWI) data of participants and used a combined diffusion tensor imaging (DTI) and generalized Q-sampling imaging (GQI; Yeh et al., 2010) approach (de Lange et al., 2023) to identify the RC hubs in a group average connectome. During a functional magnetic resonance imaging (fMRI) session, the same group of participants saw nested, hierarchically structured digit sequences. Finally, we integrated the structural and functional results using two different approaches: First, by using the structurally defined network nodes and hubs as regions of interest (ROIs) for the analysis of the subject-level fMRI data. Secondly, we analyzed the structural network centrality in areas that were identified as significant clusters in the functional whole-brain analysis to further investigate the relationship between cortical function and the underlying network structure. Both of these methods of integration define their group-wise independent variables (structural ROIs and functionally identified clusters) and subject-level dependent variables (fMRI data and structural network centrality) crossmodally, thus avoiding the problem of circularity (Kriegeskorte et al., 2009).

We had two hypotheses: processing hierarchically higher structures of the stimulus (I) involves RC hubs more than other nodes and (II) anterior and/or medial regions more than posterior and/or lateral areas of the frontal cortex.

2 | MATERIALS AND METHODS

2.1 | Participants

Data of 48 right-handed participants (32 females, $M = 21.75$, $SD = 2.74$ years; range = 18–28 years) were collected in this study. Four participants had to be excluded due to technical difficulties. Additional participants had to be excluded due to an inadequate performance in the experiment (one participant) or movement during the experiment that exceeded 1.5 times the voxel size (3.3 mm) in one direction within a run (three participants). Consequently, $N = 40$ (29 females, $M = 21.73$, $SD = 2.75$ years; range = 18–28 years) subjects were included in the analysis. All subjects gave informed written consent approved by the University of Münster Research Ethics Committee in accordance with the declaration of Helsinki. None of the participants reported any history of neurological or psychiatric diseases or any ferromagnetic material inside their bodies. Participants had (corrected-to-) normal vision and were right-handed ($M = 84.85$, $SD = 16.07$, range = 30–100) as assessed by the Edinburgh Handedness Inventory (Oldfield, 1971). They received money or course credit as remuneration for participating in the experiment.

2.2 | Stimuli

Subjects were presented with sequences of digits made up of the numbers 4, 5, 6, 7, 8, 9, and 0 (for task instructions, see Section 2.3). Digits 1–3 were excluded due to evidence for different neural processing of these numbers in humans (Goffin, 2019). Importantly, only one digit was presented on screen at a time. The nested digit sequences were constructed from chunks of subsequently presented digits of varying length depending on the experimental condition (see below). Additionally, digit sequences were pseudorandomly interrupted by targets which required a response (button press) by the participants to ensure their constant attention. Target trials were characterized by the presentation of the number zero due to this digit's special role on the number scale (Brysbaert, 1995; Nieder, 2016; Pinhas & Tzelgov, 2012).

The experimental design comprised four conditions: (1) *Single*, where the transition probability between all digits was equal (i.e., no digit allowed an above-chance prediction of the subsequent one); (2) *Triplet*, in which the digits appeared in predefined chunks of 3 (4-5-6, 6-5-4, 7-8-9, and 9-8-7); (3) *Nonet*, with predefined chunks of nine digits created by repeating a triplet three times each (4-5-6-4-5-6-4-5-6, 6-5-4-6-5-4-6-5-4, 7-8-9-7-8-9-7-8-9 and 9-8-7-9-8-7-9-8-7); and finally (4) *Complete*, where subjects were presented with the complete sequence of 36 numbers the other conditions were nested in (4-5-6-4-5-6-4-5-6-6-5-4-6-5-4-6-5-4-9-8-7-9-8-7-9-8-7-7-8-9-7-8-9-7-8-9) (Figure 1a). The nested hierarchy of this sequence was chosen to resemble the structure and subsequent division of the natural stimuli used previously to analyze temporal receptive windows (TRW; Farbood et al., 2015; Hasson et al., 2008, 2010; Lerner et al., 2011). Each condition was presented five times during

the main experiment (divided into 20 experimental blocks with one condition presented per block) and once each during a preceding training session.

Transition probabilities of Single digits, Triplet, and Nonet chunks were balanced using concatenated de Bruijn sequences of the order of two (de Bruijn, 1946), creating ideal pseudorandom sequences (Aguirre et al., 2011) of 144 digits. Each sequence was completed by 18 pseudorandomly inserted zeros (targets), which occurred at 12.5% of transitions on a chunk level, and neither in the first three trials of each block nor in direct succession. For each condition, six different digit sequences were created. Then, these unique sequences were randomly assigned to each training and experimental block to avoid the repetition of sequences within the same condition. The creation of all digit sequences and balancing of transition probabilities was done using MATLAB (Version 9.6.0 [R2019a]; The MathWorks Inc., 2019). For the creation of the de Bruijn sequences, we used the MATLAB-based de Bruijn sequence generator (Brimijoin & O'Neill, 2010).

Stimuli were presented using Neurobs Presentation software (Version 20.3, Neurobehavioral Systems, Inc., Berkeley, CA, www.neurobs.com). “Microsoft JhengHei Light” was chosen as the font as it represented the best balance between readability and minimization of relative pixel overlap (Wong & Szűcs, 2013). Digits were presented at a visual angle of approximately 1.29° in very light gray, RGB = (230, 230, 230), on a dark gray background, RGB = (40, 40, 40).

2.3 | Procedure

The experiment was divided into two sessions in the MRI scanner that were completed on two separate days: the fMRI-task day and the

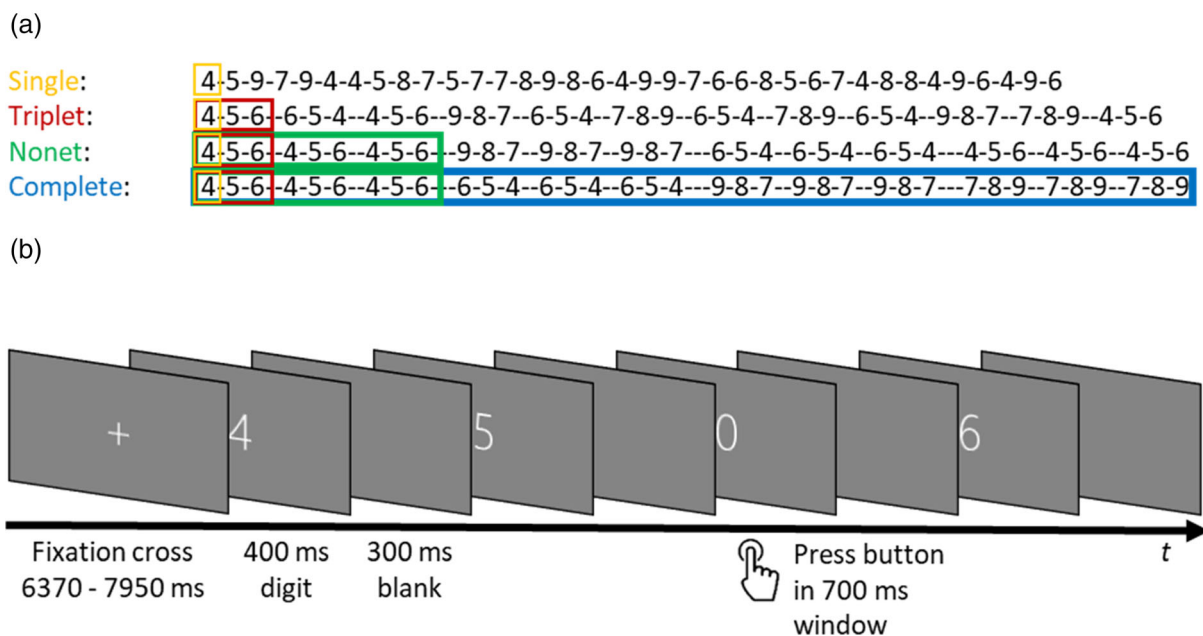


FIGURE 1 Experimental paradigm on the functional magnetic resonance imaging (fMRI)-experiment day. Example sequences for the four conditions. (a) Colors show nested hierarchical structure. (b) Presentation of digit sequence. Participants had to press a button when a zero was presented.

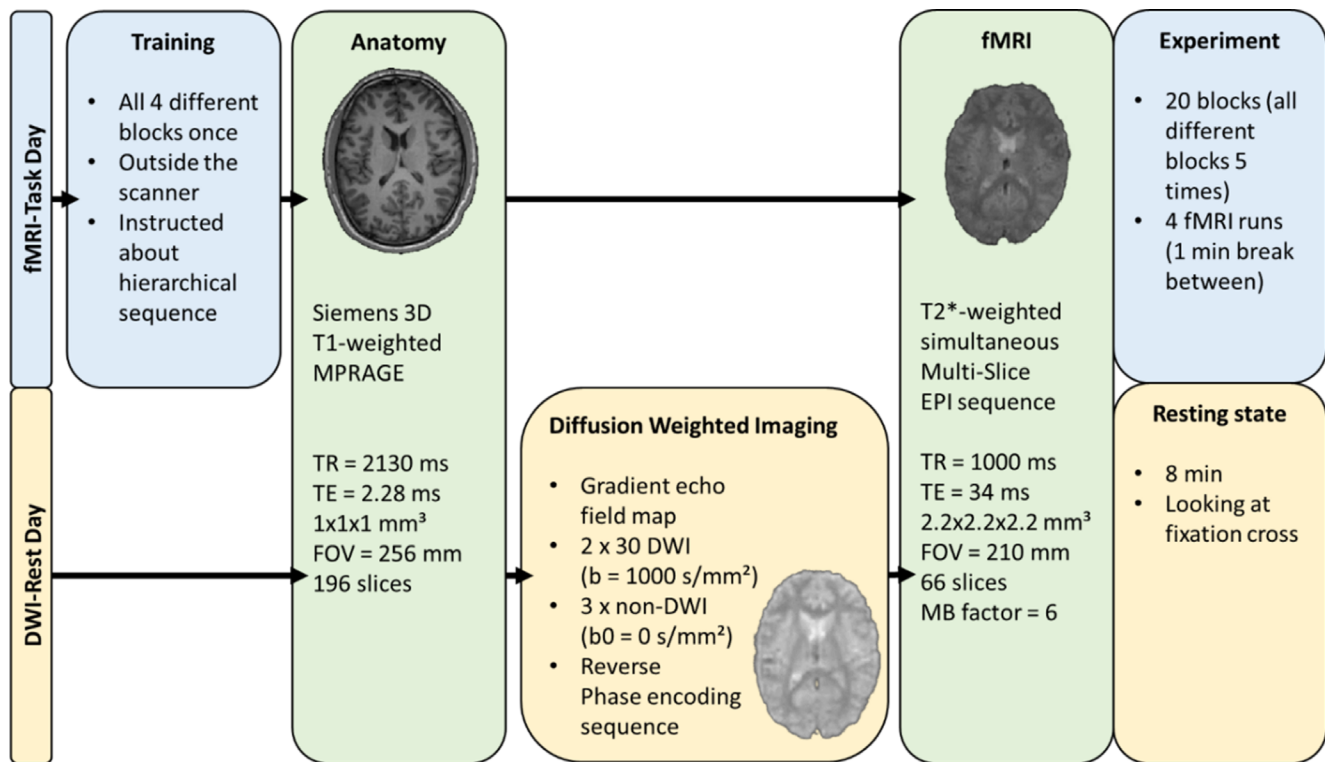


FIGURE 2 Diagram of the experimental procedure. DWI, diffusion weighted imaging; EPI, echo planar imaging; FOV, field of view; MB, multiband; MPRAGE, magnetization prepared rapid acquisition gradient echo; TE, echo time; TR, time of repetition. Note that the order of the two sessions (functional magnetic resonance imaging [fMRI]-task and DWI-rest) were counterbalanced across participants.

DWI-rest day (Figure 2). The order of sessions was counterbalanced across the group. On average 7.58 days ($SD = 6.05$ days) passed between sessions.

On the fMRI-task day, participants saw 24 blocks of the digit task, four blocks in the training outside the scanner, and then 20 blocks during the experiment in the MR scanner. Every participant was assigned a different order of blocks, with the first blocks in training and the main experiment counterbalanced across participants between the four conditions. The training (including all four conditions) and the main experiment started with the same condition. The block order was pseudorandomized using adjusted de Brijn sequences to control that the transition probabilities between each condition were the same, but two blocks of the same condition could never be presented directly after each other. Each of the four blocks of the training and the 20 blocks of the main experiment consisted of 162 trials in total. At the start of each block, a fixation cross was presented for a block-specific jittered duration of 6370–7950 ms. The fixation cross blinked three times in the rhythm of number presentation signaling the approaching start of the next block. Each trial took 700 ms, consisting of a 400 ms digit presentation followed by 300 ms of a blank screen. If a zero was presented, the participant had the whole 700 ms to press the response button with the right index finger (Figure 1b). The experiment continued regardless of the response without feedback. Additionally, the main experiment contained a break of 1 after every five blocks, where the participants were informed about their progress in the experiment. To motivate

participants, they could earn extra money/course credit when they responded to the zeros. At the end of the experiment, they were notified about the amount of additional reward they won. In total, the participants spend approximately 60 min in the scanner during the fMRI-task day.

For the DWI-rest day, measurements included an anatomical T1-weighted image (approx. 5 min), multiple diffusion-weighted (DW) images and non-DW images (approx. 15 min; see Section 2.4) and a resting-state fMRI scan (approx. 8 min). Participants were asked to remain as still as possible for the duration of the measurements. We presented the participants with a fixation cross during the resting-state fMRI scans, which is recommended for resting-state measurement (Agcaoglu et al., 2019; Patriat et al., 2013; van Dijk et al., 2010). The total scanner time on the DWI-rest day was about 30 min.

All stimuli were projected on a screen that was positioned behind the scanner bore. Participants viewed the screen via an adjustable 45° mirror. Movements were minimized with form-fitting cushions. To reduce scanner noise, ear plugs and noise-cancelling headphones were provided.

2.4 | MRI data acquisition

Brain images were recorded with a 3 T Siemens Magnetom scanner (Siemens, Erlangen) using a 20-channel head coil. Functional blood-

oxygen-level-dependent (BOLD) images on both days were acquired parallel to the anterior commissure/posterior commissure line. We used a T2*-weighted simultaneous multi-slice echo-planar imaging (SMS-EPI; 94×94 data acquisition matrix; 210 mm field of view [FOV]; 57° flip angle; time of repetition [TR] = 1000 ms; echo time [TE] = 34 ms). Each volume consisted of 66 adjacent axial slices with a slice thickness of 2.2 mm, a gap of 0.11 mm (5%), and a voxel size of $2.2 \times 2.2 \times 2.2$ mm³. Slice acquisition and multislice mode were interleaved. The acceleration factor was 6. The functional acquisition on the fMRI-task day was completed in four runs between which the participants had a 1-min break.

Structural reference images during both days were acquired for each participant using a standard Siemens 3D T1-weighted MPRAGE sequence for a detailed reconstruction of anatomy with isotropic voxel size ($1 \times 1 \times 1$ mm) in a 256-mm FOV (256×256 matrix; 192 slices; 8° flip angle; TR = 2130 ms; TE = 2.28 ms).

For DWI, we applied the parameters of the imaging sequences used in the Marburg-Münster Affective Disorders Cohort Study (Vogelbacher et al., 2018). Imaging started with a gradient echo field map (320 mm FOV; 60° flip angle; TR = 616 ms; TE1 = 5.19 ms; TE2 = 7.65 ms; 56 slices, slice thickness = 2.5 mm; 0 mm gap; voxel size $2.5 \times 2.5 \times 2.5$ mm³; interleaved slice acquisition). This was followed by two times 30 DW images with a *b*-value of 1000 s/mm² and in total five non-DW images (*b* = 0 s/mm²), that had the same parameters except for their *b*-value (320 mm FOV; initial rotation -90° ; TR = 7300 ms; TE = 90 ms; 56 slices, slice thickness = 2.5 mm; 0 mm gap; voxel size = $2.5 \times 2.5 \times 2.5$ mm³; interleaved slice acquisition; GRAPPA acceleration factor = 2). DWI was completed by a reverse phase encoding sequence (320 mm FOV; initial rotation -90° ; TR = 7300 ms; TE = 90 ms; 56 slices, slice thickness = 2.5 mm; 0 mm gap; voxel size = $2.5 \times 2.5 \times 2.5$ mm³; interleaved slice acquisition; GRAPPA acceleration factor = 2).

2.5 | fMRI preprocessing

Preprocessing of functional and anatomical data was performed using the Statistical Parametric Mapping software (SPM12; The Wellcome Centre for Human Neuroimaging, London, UK) implemented in MATLAB (Version 9.10.0 [R2021a]; The MathWorks Inc., 2021). Preprocessing included manual reorientation to MNI space (Montreal Neurological Institute, Montreal, QC, Canada), slice time correction to the temporal and spatial middle slice (slice 34), realignment to the mean EPI image, and co-registration of the functional images to the individual structural scans. The subjects' co-registered anatomical (T1) scans were then segmented into native space tissue components. To this end, we used DARTEL (Ashburner, 2007) implemented in SPM12 with the default settings to create a group-specific template. Individually created flow fields were then used to normalize the functional images to MNI space. Finally, a Gaussian kernel of 8 mm³ full-width at half-maximum was applied by DARTEL to smooth the data. A 160 s temporal high-pass filter was applied to remove low-frequency noise from the functional images' timeseries. To pre-whiten the data

and correct for temporal autocorrelations, we applied the FAST model as recommended for TR \leq 1400 ms (Corbin et al., 2018).

2.6 | Network reconstruction

To be able to analyze the structural network of the brain, the white matter network has to be reconstructed from the DW images to then determine the structural connectivity matrix describing this network. This reconstruction of the DWI-based structural connectivity matrices was done with the Connectivity Analysis Toolbox (CATO, v3.1.2.; de Lange et al., 2023). To this end, additional (preprocessing) steps had to be performed on the anatomical (T1) and DW images.

First, cortical surface reconstruction from the T1 images was performed using recon-all from FreeSurfer (v7.2.0; Fischl, 2012). This processing step was necessary as the T1 images are captured in voxels that do not directly contain the information of the brain's location and surface structure. It also included the automatic parcellation of the brain's surface according to the Desikan-Killiany atlas (Desikan et al., 2006). To ensure the quality of the anatomical reconstruction and parcellation, we applied the quality control protocol used by the ENIGMA consortium (<https://enigma.ini.usc.edu/>). Thus, we extracted the cortical thickness (in mm) and the surface area (in mm²) of every parcel according to the Desikan-Killiany atlas of each participant to identify outliers, which might indicate issues in the parcellation but could also just reflect anatomical variability. Then, the parceled cortical surfaces of every subject were visually inspected internally, for accurate segmentation between gray and white matter and tracing of sulci, and externally, for successful differentiation of areas, and for general parcellation errors by one of the authors (FM) and three student assistants. No participants had to be excluded based on the results of this quality control. Thus, we ended up with parcellated cortical surfaces of all 40 participants.

Second, to merge the 60 DW and five *b*₀ images per participant, we used fslmerge from FSL 6.0 (Jenkinson et al., 2012; CATO uses FSL to prepare the DWI data). The pipeline included a susceptibility correction using FSL topup (Andersson et al., 2003; Smith et al., 2004) based on the recorded Reverse Phase Encoding images and an eddy current as well as movement correction using FSL's eddy (Andersson & Sotiropoulos, 2016). For the reconstruction of the anatomical network, CATO allowed us to use a combined method of DTI and GQI (Yeh et al., 2010). Thus, in cases of multiple diffusion peaks because of more complex fiber configurations (e.g., kissing or crossing fibers), the voxel-wise diffusion profiles were determined using GQI. Otherwise, the informed RESTORE algorithm (Chang et al., 2005, 2012) was applied to model the tensor and remove outliers during the fitting, which helps with reducing the influence of physiological noise on the DTI modeling. Following the reconstruction of the diffusion signal, white matter tracts were reconstructed using deterministic tractography. For the reconstruction of the fibers following the diffusion peaks in each voxel, the FACT algorithm (Mori et al., 1999) was applied, extended for multiple peaks. This step resulted in the estimation of every participant's white matter streamlines.

Third, for the reconstruction of the DWI-based connectivity matrices (Figure 3), we used the default settings of CATO based on van den Heuvel et al. (2013). The algorithm started with eight seeds from each voxel in the brain mask, following the main direction of the diffusion to the next voxel and stopped in one of five cases: (1) the reconstructed white matter streamline reached a voxel with a fractional anisotropy (FA) value of 0.1, which often corresponds to gray matter; (2) the streamline tried to exit the brain mask; (3) it made a sharp turn larger than 45°; (4) it revisited a previous voxel; or (5) it entered a region defined as a *forbidden region*, which describes the

cerebellum. Only streamlines that fully connected two brain regions were considered. The connectivity matrices for each participant were constructed based on a parcellation of their T1 anatomy. The parcellation of the individual anatomy in accordance with the same atlas or parcellation scheme is necessary to have an equal definition of parcels that form the nodes of the network and can be compared or combined across subjects. CATO extends on the classical Desikan–Killiany (Desikan et al., 2006) parcellation and includes the *Lausanne sub-parcellations*, which represent an approach to achieve the optimal scaling for connectivity matrices (Cammoun et al., 2012). We considered both

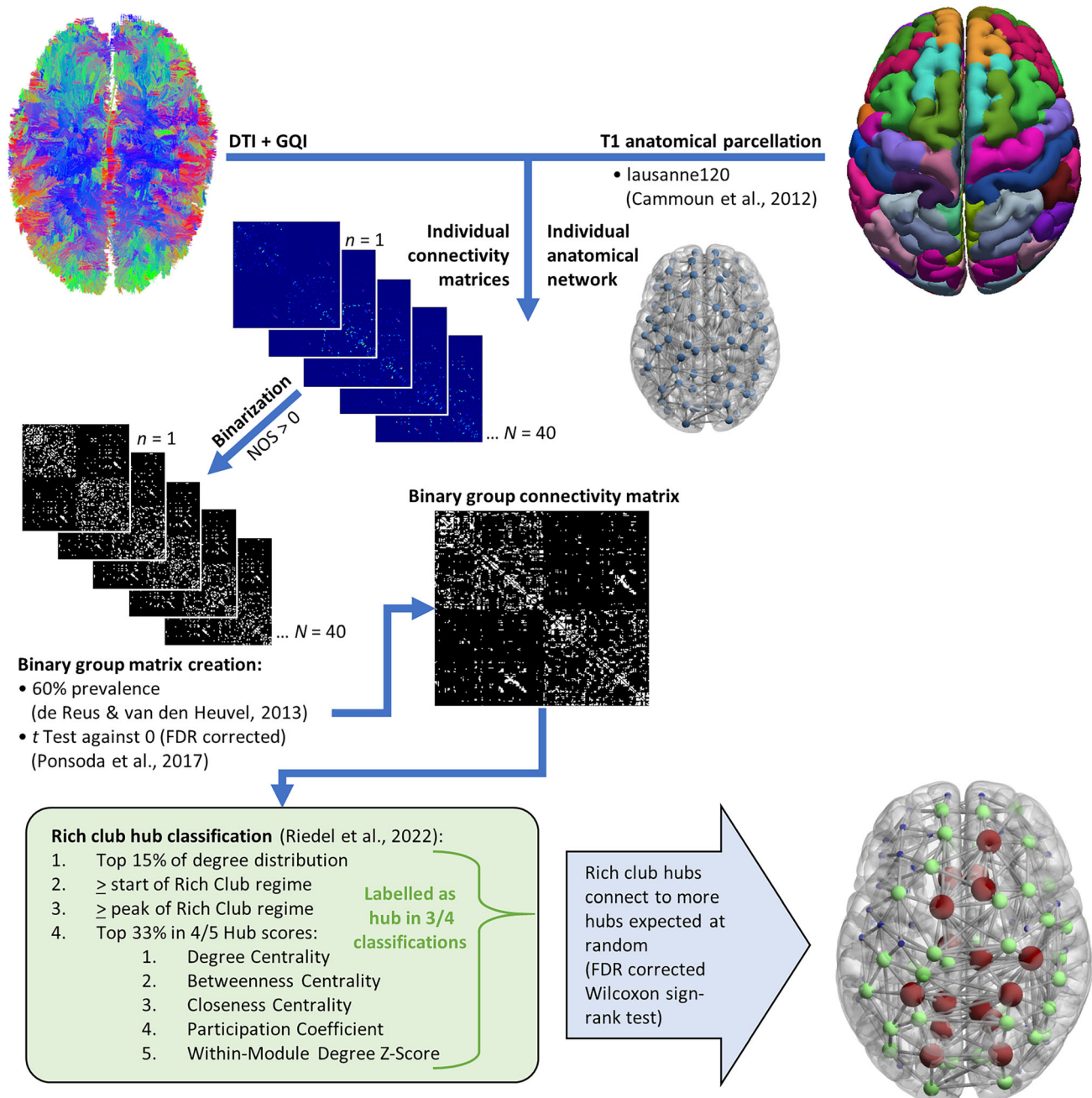


FIGURE 3 Flowchart from diffusion weighted images to rich club hubs. DTI, diffusion tensor imaging; FDR, false discovery rate; GQI, generalized Q-sampling imaging; NOS, number of streamlines.

the *lausanne120* and *lausanne250* parcellation schemes, as they showed the best reliability (Cammoun et al., 2012) and represent a meaningful meso-level parcellation of the cortex (Amunts & Zilles, 2015). The main manuscript is focused on the *lausanne120* parcellation scheme (Figure 3) while all analyses using the *lausanne250* parcellation are contained in the Supplemental Material.¹ The results according to both parcellation schemes are discussed together. The application of the *lausanne120* parcellation resulted in the construction of 114×114 connectivity matrices for each subject. Note we did not include subcortical regions, as our functional hypotheses focused on cortical areas.

Finally, as connectivity matrices tend to be sensitive to outliers (Chung et al., 2017), we controlled the quality of the connectivity matrices based on the guidelines described in van den Heuvel et al. (2019). We determined outliers based on the following matrix measures: average number of streamlines (NOS), average FA, average mean diffusivity, average length, average streamline density controlled for the volume of the connected regions (in number of voxels), and distance to group prevalence map. Outliers were identified as values either below $Q1 - 2 \times IQR$ or above $Q3 + 2 \times IQR$ ($Q1$ = first quartile, $Q3$ = third quartile, $IQR = Q3 - Q1$ = interquartile range). Only connectivity matrices of participants that showed no outlier in any of the measures were used for further analysis. No subjects had to be excluded due to this quality check of matrix norms. Consequently, the network construction resulted in an individual DTI-GQI-based weighted connectivity matrix according to the *lausanne120* parcellation scheme for all 40 participants.

2.7 | From connectivity matrices to ROIs

To investigate hypothesized relationships between hierarchies in function and structure, we identified the RC hubs of the group network and used these hubs as ROIs for the analysis of task-based BOLD data. First, we created a binary connectivity matrix for each participant (Figure 3) to reduce the bias from inaccuracies caused by the applied DWI sequence (Fornito et al., 2016). We binarized the individual DTI-GQI-based connectivity matrices by setting every edge that had at least one streamline ($NOS > 0$) to one while others were given a value of zero. These binarized matrices were then summed and thresholded in two different ways (Figure 3) that are both used to avoid false positive streamlines. The first way was based on the results of de Reus and van den Heuvel (2013a), who found that keeping connections that are present in at least 60% of the participants produces a good balance between false negative and false positive connections. The second method applied used one-tailed one-sample t tests to examine whether an edge's *relative NOS* ($NOS/\text{total NOS}$ of a given participant) was larger than zero (Ponsoda et al., 2017). T tests were then corrected for multiple comparisons using the Benjamini and Hochberg (1995) method to control the false discovery rate (FDR)

¹Note the ROI and centrality analyses results of both parcellation schemes were very similar. The decision to feature the *lausanne120* parcellation in the manuscript was made for the sake of clarity of the connectome depictions.

and adjust the p value accordingly. These two methods resulted in two different group-wise connectomes for the *lausanne120* parcellation scheme with 463 and 455 edges, respectively (Figure S5.1).

The following identification of hubs was based on the methods described in Riedel et al. (2022). In deviation from their approach, we used binarized group matrices instead of individual weighted matrices. This deviation was implemented since the individual differences in RC organization were not relevant for our purposes. Also, major structural connectivity patterns are more apparent in group-wise connectomes (Hagmann et al., 2008). The Brain Connectivity Toolbox (BCT) for MATLAB (Rubinov & Sporns, 2010) was applied to determine the RC coefficient

$$\phi(k) = \frac{2E_{>k}}{N_{>k}(N_{<k} - 1)} \quad (1)$$

(`rich_club_bu.m` from the BCT) for each node degree k . The node degree k , also called degree centrality, describes the number of edges an individual node has with other network nodes (Rubinov & Sporns, 2010). The undirected and binary RC coefficient $\phi(k)$ was then calculated as the proportion of the links between nodes with a degree higher than k divided by the total possible number of links between all nodes of this subset (van den Heuvel & Sporns, 2011). These RC coefficients were normalized by dividing them by the mean RC coefficient of 2500 random networks. The randomization was achieved by applying the `randmio_und.m` function from the BCT 2500 times to the group network, rewiring each connection ten times.

As the RC coefficient $\phi(k)$ is calculated for every node degree k , it is possible to identify a range of degrees for which the empirical RC coefficient $\phi(k)$ is significantly higher than in the random networks. This range of degrees is called the RC regime (van den Heuvel & Sporns, 2011). We used the same rules as Riedel et al. (2022) to identify the RC regime as the largest range of consecutive degrees k , for which the empirical RC coefficient was significantly larger ($\alpha = .05$) than the random coefficients. Therefore, we calculated the p values using the formula described in van den Heuvel and Sporns (2011). We adjusted for multiple comparisons by controlling the FDR.

Based on this range of k with significantly larger empirical RC coefficients $\phi(k)$, we identified individual hubs by following the criteria used in Riedel et al. (2022) (Figure 3): (a) The regions belonged to the top 15% of the degree distribution (also applied in, e.g., Liu et al., 2020; Repple et al., 2020; Yan et al., 2018). (b) The region's degree was at least as large as the start degree of the RC regime, so the first node degree k for which the empirical RC coefficient $\phi(k)$ is significantly larger than in the random networks. (c) The region's degree was at least as large as the degree k with the largest normalized RC coefficient within the RC regime. (d) The region was within the top 33% in four of the following five *hub scores*: node degree, betweenness centrality, nodal path length or closeness centrality, between-module participation coefficient, and within-module degree z -score. The calculation of modularity was done exactly as in Riedel et al. (2022) using the Louvain algorithm. Thus, we determined 100 partitions of the group network ($\gamma = 1$) with the

community_louvain.m function, found an agreement matrix of all partitions (agreement.m) and arrived at the final partition by applying consensus_und.m to threshold the agreement matrix ($\tau = .6$) applying the Louvain algorithm 100 times resulting in a single ideal community structure. In the end, we defined hubs using four different approaches.

Since the four hub definitions (a–d) produced inconsistent results, we applied additional criteria to reach a conclusive hub definition. First, we only looked at regions identified as hubs in at least three of the four hub criteria introduced above. Of these regions, only those were considered that were connected to other identified hub regions more likely than in random networks, as this is in line with the definition of the RC in general (Colizza et al., 2006). Therefore, for each identified region, we calculated the proportion of edges connecting to other identified hub regions in relation to the total degree k of that region (Figure 3). Only those regions with edge proportions significantly larger than the average edge proportions calculated from the 2500 random networks were finally labeled as RC hubs. To test the difference between empirical and random networks, we applied a Wilcoxon sign-rank test FDR corrected for multiple comparisons. This step resulted in the final set of RC hubs (Tables S6.1–S6.2).

To use the hub classification in the analysis of the task-based data, we subsequently created binary ROI maps for each parcel to extract the functional BOLD neural responses from the parcels. To create these binary ROI maps of the lausanne120 parcels, we used the *Multi-Scale Brain Parcellator* (Tourbier et al., 2019) to parcellate the MNI-152 standard template according to the lausanne120 atlas. This parcellated template was implemented as an atlas in the WFU pick atlas toolbox for SPM (Maldjian et al., 2003). In the WFU pick atlas toolbox we could make use of the *DILATE* option to dilate the only surface-level defined ROIs by one voxel size three-dimensionally as it is commonly applied when combining fMRI and diffusion-based tractography (Jarret et al., 2022). So, each of the 114 cortical areas could be extracted as an ROI. We categorized each network node and thereby ROI as RC, which is an area identified as an RC hub, or *Feeder*, which is an area that is not itself an RC hub but shares a direct edge with a RC hub in the binary group network underlying this classification, or *Local*, an area that neither belongs to nor is connected to the RC (Figure 4 and Tables S6.5–S6.6). This classification was later used for the ROI and centrality analyses (see Sections 2.8.3 and 2.8.4).

2.8 | Statistical data analysis

2.8.1 | Behavioral analysis

The behavioral and all other data analyses were performed using R (Version 4.2.2.; R Core Team, 2022) and RStudio (Version 2022.7.2.576; RStudio Team, 2022).

Reaction time

We expected a main effect of the different conditions on reaction times (RTs). Specifically, RTs in the Single condition were expected to

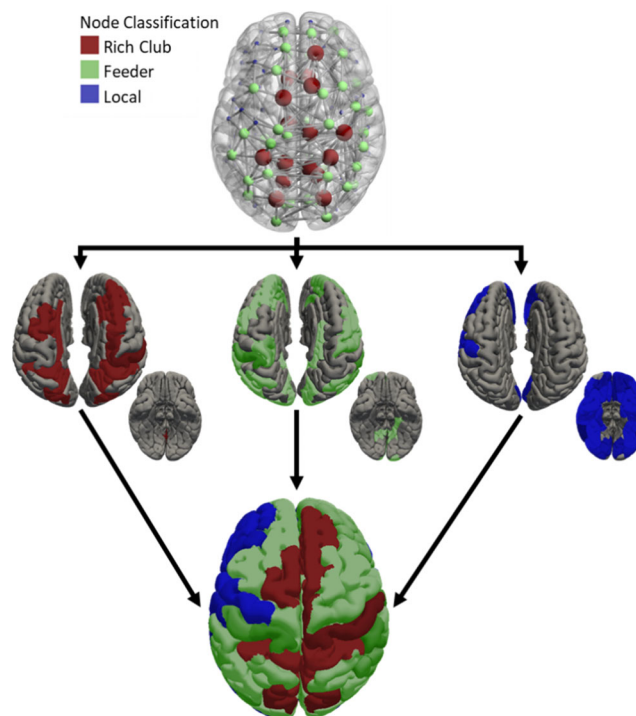


FIGURE 4 Transition from network node classification to regions of interest in MNI space. Rich Club = area is an identified rich club hub, Feeder = area directly connect to a rich club hub, Local = areas neither part of, nor connection to a rich club hub. MNI, Montreal Neurological Institute.

be shorter than in the structured conditions because expectation violations were found to lengthen RTs (Badre & Wagner, 2004; Kühn & Schubotz, 2012; Nattkemper & Prinz, 1997). Accordingly, it was also to be expected that zeros appearing within a sequential structure would lead to longer RTs than those appearing between sequence transitions. To investigate this assumption, we applied Bayesian hierarchical generalized linear modeling implemented via the brms library in R (Bürkner, 2017) to model the influence of the different blocked conditions and the level of structure disruption. HIERARCHY, a four-level within-subject factor, was comprised of the different conditions of hierarchy: Single, Triplet, Nonet, and Complete. The second factor, LEVEL OF VIOLATION, referred to where in the sequential structure a zero occurred; this factor also had four levels: *Between Single*, *Between Triplet*, *Between Nonet*, and *Between Complete*. However, the levels of the two factors were not fully crossed, as not all levels of violation could occur at each level of HIERARCHY. Thus, we used two different models (Equations 2 and 3) to investigate the influence of sequential structure on the RT. Both models included a random intercept and random slopes for the trial number, the trial number in the block, the times the participant saw this condition already to control for learning and tiredness as well as the distance of a zero to the last recorded reaction and the Shannon surprise (Shannon, 1948) of that zero in the sequence up to this point. The second model also included a random slope for the factor HIERARCHY. The surprise of a stimulus was calculated using the formula derived from the infinite time scale model (Harrison

TABLE 1 Average hit rates and false alarm rates of reacting to zeros in the digit sequences.

Hit rate LEVEL OF VIOLATION	HIERARCHY			
	Single	Triplet	Nonet	Complete
Between Single	97.61 (3.30)	97.54 (3.81)	97.47 (4.97)	97.57 (3.29)
Between Triplet		97.91 (3.25)	97.53 (4.44)	97.25 (4.76)
Between Nonet			98.00 (4.64)	97.46 (7.36)
Between Complete				100.00 (0.00)
False alarm rate	0.07 (0.16)	0.07 (0.10)	0.10 (0.15)	0.12 (0.20)

Note: Reported is $M(SD)$ in %, $N = 40$.

et al., 2006). This variable was used as part of the random structure in our models. See Supplemental Material for details on the calculation of surprise.

For the first model, we combined HIERARCHY and LEVEL OF VIOLATION to the factor COMBINATION to model the mean RT for each possible combination of the two factors.

$$RT \sim \text{Combination} + (1 + \text{Trial Number Total} + \text{Trial Number Block} + \text{Times Block} + \text{Last Zero} + \text{Surprise} | \text{Subject}) \quad (2)$$

The data for the second model than excluded the Single condition and added the factor POSITION, which was labeled *Between* for a violation during the transition of the condition-specific highest chunk (e.g., insertion between triplets in the Triplet condition) while *Within* described all other positions in the sequence. Thus, we could model an interaction effect between HIERARCHY and POSITION.

$$RT \sim \text{Hierarchy} \times \text{Position} + (1 + \text{Hierarchy} + \text{Trial Number Total} + \text{Trial Number Block} + \text{Times Block} + \text{Last Zero} + \text{Surprise} | \text{Subject}) \quad (3)$$

We used uninformative priors for both models as recommended for multilevel modeling (Bürkner, 2017). For β coefficients we used $N(0, 5)$; for the standard deviation a Student's $t(3, 0, 5)$ distribution was applied; and finally for the correlation in Equation 3, a Lewandowski-Kurowicka-Joe (LKJ(2)) distribution was used. For both models, we used the shifted lognormal family. The RT models were calculated with ten chains, each with 4000 iterations from which the first 1000 were warmups.

Hit rate

Due to the apparent ceiling effect (Table 1) and its effect on the statistical analysis (Cramer & Howitt, 2011; Rhodes et al., 2019), we only descriptively report the hit and false alarm rates of HIERARCHY and LEVEL OF VIOLATION and refrain from further analyses.

2.8.2 | fMRI design specifications

The whole brain analysis and extraction of data for the ROI analysis were conducted in the SPM12. A general linear model (GLM) was

used to model the fMRI timeseries on the first level. The GLM included four regressors for each of the different blocked conditions: Single, Triplet, Nonet, and Complete. These regressors were modeled as epochs with a duration of 162 trials (entire block duration). The onsets were time-locked to the start of the blocks, resulting in five onsets per condition. We further included the fixation epochs, the 360 events of a zero interrupting the digit sequence, and six rigid-body transformations (regressors of nuisance). Regressors were convolved with the canonical hemodynamic response function.

To identify areas that process hierarchically lower or higher structures in the digits sequence, we built contrasts between the four levels of HIERARCHY: Triplet > Single, Nonet > Triplet, and Complete > Nonet. On the second level, we applied one-sample t tests across the participants. For the particular contrasts of interest, we employed a cluster-forming threshold of $p < .001$ and a cluster extend threshold of 47 voxels. This cluster threshold was determined by 10,000 Monte Carlo simulations and represents a cluster-wise $p < .05$ corrected for multiple comparisons (Slotnick, 2017; Slotnick et al., 2003; for simulation results, see Supplemental Material).

Finally, to specifically test for the predicted anterior-medial trend in the frontal lobe for the processing of hierarchically higher stimulus structures, we computed the correlations between the Euclidian distance to an anterior-medial reference point, $X_{MNI} = 0$, $Y_{MNI} = 72$, and the extracted beta values of the step-wise contrasts from the frontal lobe. Using the Hittner et al. (2003) modification of the z test by Dunn and Clark (1969) within the cocor framework (Diedenhofen & Musch, 2015), we then compared the contrast-specific correlations to see if the beta values increase or decrease differently with distance from the anterior-medial reference point (for more details see Supplemental Material). For higher-level contrasts, we expected larger beta values to be located closer to the anterior-medial reference point while for lower-level contrasts the beta values should increase with the distance. Consequently, the correlations of higher-level contrasts should be smaller than in lower levels.

2.8.3 | ROI analysis

In preparation for the ROI analyses, we used the same GLM to estimate the mean activations per condition by calculating the contrast of the respective condition against the implicit baseline, which is the predicted BOLD activation when all predictors are set to zero. Then we

extracted the unthresholded, estimated beta values from the contrast images for each ROI per level of HIERARCHY in each participant, using the `spm_get_data.m` function from the SPM12. We subsequently averaged the beta values from all voxels of an ROI for every level of HIERARCHY and participant. ROIs were grouped into RC hubs, Feeder nodes, and Local nodes, depending on their RC membership and connectivity. The extraction and classification were done for both group network construction methods. After inspection of the Cullen–Frey plots, to judge the skewness and kurtosis of the data (Cullen & Frey, 1999), extreme averaged beta values (below $Q1 - 3 \times IQR$ or above $Q3 + 3 \times IQR$) were excluded from the analysis.

The statistical ROI analysis was performed using Bayesian hierarchical generalized linear models via the `brms` package (Bürkner, 2017). In the model, HIERARCHY, NODE CLASSIFICATION, and the HIERARCHY by NODE CLASSIFICATION interaction were included as predictors. The model also incorporated random intercepts for the individual ROIs, subjects, and a random HIERARCHY effect for each subject (Equation 4).

$$\text{Beta} \sim \text{Hierarchy} \times \text{Node Classification} + (1 + \text{Hierarchy} | \text{Subject}) + (1 | \text{ROI}) \quad (4)$$

As the model was multilevel, we used the same priors as for the behavioral data (see “Reaction Time” section). The skewed normal family was utilized for modeling the data. All models were calculated with ten chains, each having 4000 iterations, 1000 warmups, and a maximal treedepth of 15.

We hypothesized that the RC hubs would be more activated in conditions that involve the processing of hierarchically higher stimulus structures. Thus, the interaction between HIERARCHY and NODE CLASSIFICATION was of particular interest, as beta values should increase significantly with hierarchically higher structures. This was especially expected in areas identified as RC hub regions, and possibly also in Feeder nodes which are (by definition) directly connected to the RC.

2.8.4 | Centrality analysis

We then examined the graph theoretical node properties of the areas with hierarchal level-specific BOLD responses. Again, we assumed that areas that process hierarchically higher structures of the stimulus also occupy hierarchically higher levels in the structural graph, which are more central to the network.

First, we started with using the already established individual DTI-GQI-based connectivity matrices referenced to the lausanne120 parcellation scheme before the merging to group-wise matrices (see Section 2.6). To be able to use the binarized matrices on a subject-level, we applied a different binarization method than on the group-level. At the individual level we fixed the threshold for keeping an edge at three or more streamlines to correct for false positives (Brown et al., 2011), setting edges clearing this threshold to one and all others to zero. Based on these individual binary connectivity matrices, we calculated the five centrality measures that make up the hub score in the RC identification (Riedel et al., 2022) for each individual network: nodal degree/degree centrality, betweenness centrality,

closeness centrality, within module degree z-score, and participation coefficient.

Second, we used the resulting clusters of the group-averaged BOLD contrasts Triplet > Single, Nonet > Triplet, and Complete > Nonet that were significant at the cluster threshold of 47 voxels (Table 3 and Figure S5.2) as functional ROIs and extracted them binarized maps.

Third, based on these maps, we assigned the functionally defined *Rhat* activation clusters to parcels of the lausanne120 atlas (see Supplemental Material for lausanne250). Therefore, we calculated the proportion of each binarized functional cluster that was contained in the parcels of the lausanne120 parcellation scheme. As a result, we determined the lausanne120 parcels that comprised activations of the Triplet > Single, Nonet > Triplet, and Complete > Nonet contrasts as well as a percentage of the contrasts contained in each of these parcels.

Fourth, for each of the three BOLD contrasts, we then determined the weighted average for all five node centralities, weighted by the percentage of overlap between contrasts and parcel.

We repeated this step for each subject to receive individual structural centrality measures based on the subject's binary network for all clusters of the functional analysis. These individual measures were also controlled for the total amount of activated voxels of a contrast covered by any parcel. This culminated in five controlled centrality measures for each of the stepwise contrasts for all 40 participants. Finally, we z-scaled every centrality measure to obtain comparable values for all five measures.

To analyze the difference between the mean centrality of the stepwise contrasts we applied a multivariate multilevel model via `brms` (Bürkner, 2017) with the factor HIERARCHY CONTRAST describing the influence of the different levels of contrasts (Equation 5).

$$\begin{aligned} &(\text{Degree Centrality, Betweenness Centrality, Closeness Centrality,} \\ &\text{Within Module Degree z-Score, Participation Coefficient}) \sim \quad (5) \\ &\text{Hierarchy Contrast} + (1 | \text{Subject}) \end{aligned}$$

We expected that the average centrality of the areas activated by hierarchically higher structures of the stimulus would increase with the levels of hierarchy.

2.8.5 | Validation using the human connectome project dataset

As this article is the first to apply the additional step of using the connections between hub regions as a criterium for RC hub definition, we sought to validate the results of the node classification as well as the subsequent ROI and the centrality analyses on an independent dataset. For this purpose, we made use of the publicly available data from the Human Connectome Project (HCP; Van Essen et al., 2013; for details see Supplemental Material). We applied the exact same methods described in Sections 2.6–2.8.4 to the structural and DW data of 100 unrelated subjects from the HCP database. The resulting node classification was compared to the results of our own data.

Subsequently, the HCP-based classifications and structural centrality measures were utilized to replicate the ROI and centrality analyses.

2.8.6 | Bayesian hypothesis testing

The hypotheses for the Bayesian multilevel models were tested using the hypothesis function from the *brms* library (Bürkner, 2017). A Bayes factors (BF) > 3 indicates significant evidence in favor of the tested hypothesis (van Doorn et al., 2021). Bayes factors for one-sided hypotheses (BF_{+0}) are defined as the division of the posterior probability of the hypothesis by the posterior probability of the alternative, that is, the evidence ratio (Bürkner, 2018).

3 | RESULTS

3.1 | Behavioral results

3.1.1 | Hit and false alarm rates

Table 1 reports hit rates and false alarms rate in detecting the zero broken down by HIERARCHY and LEVEL OF VIOLATION only for hit rates.

3.1.2 | Reaction times

The RT model (Equation 2) tested the influence of all combinations of HIERARCHY and LEVEL OF VIOLATION on the RT for detecting a zero, controlled for participant-specific effects of learning, tiredness, and surprise. The model had no divergent transitions, all $Rhat < 1.05$, and all variables had bulk- and tail-effective samples ≥ 1373 and ≥ 2665 , respectively. Posterior checks showed that the cumulative count model simulations reasonably capture the means and distributions of the observed data (Figure S7.1). Posteriors drawn from the estimated model (Equation 2) were used to compare the RT between the levels

of HIERARCHY per LEVEL OF VIOLATION. As aforementioned, we expected that a zero inserted within the sequence would be slower than a zero presented between chunks of the sequence. It was found that the RT for a zero occurring Between Single was increased for Nonet condition in comparison to the Single condition (H_{+} : *Nonet:Between Single > Single:Between Single*; $M = 0.02$ [0.01, 0.04], $SD = 0.01$, $p.p. = 1$, $BF_{+0} = 217.98$; Figure 5a).

The second RT model (Equation 3) focused on the structured conditions to test the influence of HIERARCHY, POSITION (i.e., if the zero was inserted within or between the sequences), and their interaction on the RT. This model also had no divergent transitions, all $Rhat = 1.00$, and all variables had bulk- and tail-effective samples ≥ 2133 and ≥ 4822 , respectively. Posterior checks again showed that the cumulative count model simulations reasonably capture the means and distributions of the observed data (Figure S7.2). Posteriors drawn from the estimated model (Equation 3) revealed a larger RT in the Within position compared to the Between position in the Nonet condition (H_{+} : *Nonet:Between - Nonet:Within < 0*; $M = -0.04$ [-0.07, -0.02], $SD = 0.02$, $p.p. = 1$, $BF_{+0} = 308.28$; Figure 5b). This difference was also larger than in the Triplet condition (H_{+} : *Triplet:(Within > Between) - Nonet:(Within > Between) < 0*; $M = -0.04$ [-0.07, -0.01], $SD = 0.02$, $p.p. = 0.98$, $BF_{+0} = 58.06$; Figure 5b). These results show a tendency for a larger influence of the interruption and position of insertion on the RT with stimuli containing hierarchically higher structures. The results of the Complete condition break this pattern (H_{+} : *Nonet:(Within > Between) - Complete:(Within > Between) < 0*; $M = 0.07$ [0.01, 0.12], $SD = 0.03$, $p.p. = 0.02$, $BF_{+0} = 0.02$; Figure 5b). However, it must be noted, that the participants saw far fewer Between Complete insertions (3 per participant) than Between Nonet insertions (18 per participant).

3.2 | fMRI results

According to the hypothesis of a stepwise increase of the activation with the nested levels of hierarchy in the stimulus structure, we

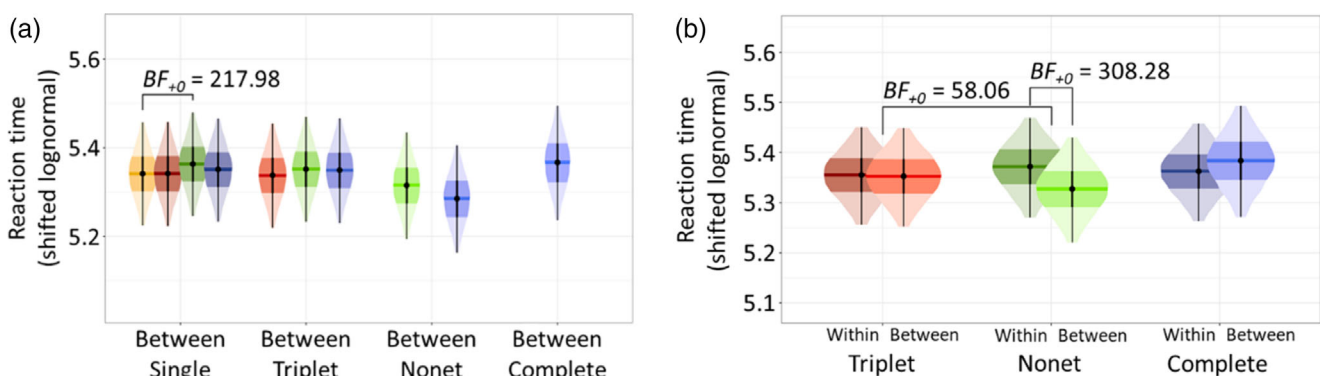


FIGURE 5 Results of reaction time analysis. Density plots of posterior distributions with mean point estimate, 50 and 95% highest probability density areas marked. BF, Bayes factor. (a) Estimates of all conditions of the HIERARCHY \times LEVEL OF VIOLATION interaction. Yellow, Single; Red, Triplet; Green, Nonet; Blue, Complete. (b) Interaction of HIERARCHY \times POSITION in structured conditions. Red, Triplet; Green, Nonet; Blue, Complete; Dark, Within; Light, Between.

examined the significant clusters at a cluster threshold of 47 voxels that was determined using the simulation introduced by Slotnick et al. (2003); Slotnick (2017). This approach revealed activation clusters for the contrasts Triplet > Single and Nonet > Triplet (Table 2 and Figure 6, for a graphic depicting all clusters see Figure S5.2). Because of their stepwise nature, we will also refer to these contrasts as Triplet-specific and Nonet-specific, respectively. The Triplet > Single contrast comprised a single cluster in the left inferior frontal junction (IFJ). The Nonet > Triplet contrast showed additional frontal clusters in right middle frontal gyrus (MFG) and two separate clusters in the right superior frontal gyrus (SFG). In the temporal lobe, we found clusters in the left inferior temporal sulcus and a cluster in the right middle temporal gyrus. Finally, we also found bilateral clusters in the inferior parietal lobule (IPL) and a cluster in the right posterior cingulate gyrus

(PCG). No significant clusters were revealed in the Complete > Nonet contrast. Activation clusters resulting from the stepwise comparison of the increasing hierarchical structure were later used as the basis for the analysis of the centrality measures (see Section 3.5).

To test for the predicted anterior-medial trend in the frontal lobe, we compared the correlations between the Euclidian distance to the anterior-frontal reference point, $X_{MNI} = 0$, $Y_{MNI} = 72$, and the extracted beta values of the Triplet > Single and Nonet > Triplet contrasts. We found that the correlations for the Nonet-specific betas, $r_{EdN} = -.07$, $t(2020557) = -97.81$, $p < .001$, as well as the Triplet-specific betas with the Euclidian distance were significantly different from zero, $r_{EdT} = .09$, $t(2020557) = 122.88$, $p < .001$. Additionally, the Nonet-specific correlation was significantly smaller than the Triplet-specific correlation, $z = -126.60$, $p < .001$. Accordingly,

TABLE 2 Activation clusters from second-level whole-brain block contrasts with cluster threshold = 47 voxels.

Localization	H	Cluster extent (in voxel)	MNI coordinates			t Value	p Value
			x	y	z		
<i>Nonet > Triplet</i>							
Superior frontal gyrus	R	73	22	60	14	3.80	<.001
Superior frontal gyrus	R	401	22	18	58	4.32	<.001
Medial superior frontal gyrus	R	l.m.	12	36	42	4.01	<.001
Superior frontal gyrus	R	l.m.	22	32	56	3.96	<.001
Middle frontal gyrus	R	108	38	24	40	4.08	<.001
Inferior temporal sulcus	L	144	-56	-24	-26	5.51	<.001
Middle temporal gyrus	R	123	64	-30	-16	3.95	<.001
Posterior cingulate gyrus	R	101	4	-40	28	4.04	<.001
Inferior parietal lobule	L	118	-54	-58	44	4.14	<.001
	R	190	44	-62	36	4.10	<.001
<i>Triplet > Single</i>							
Inferior frontal junction	L	77	-36	0	28	3.91	<.001

Abbreviations: H, hemisphere; L, left; l.m., local maximum; MNI, Montreal Neurological Institute; R, right.

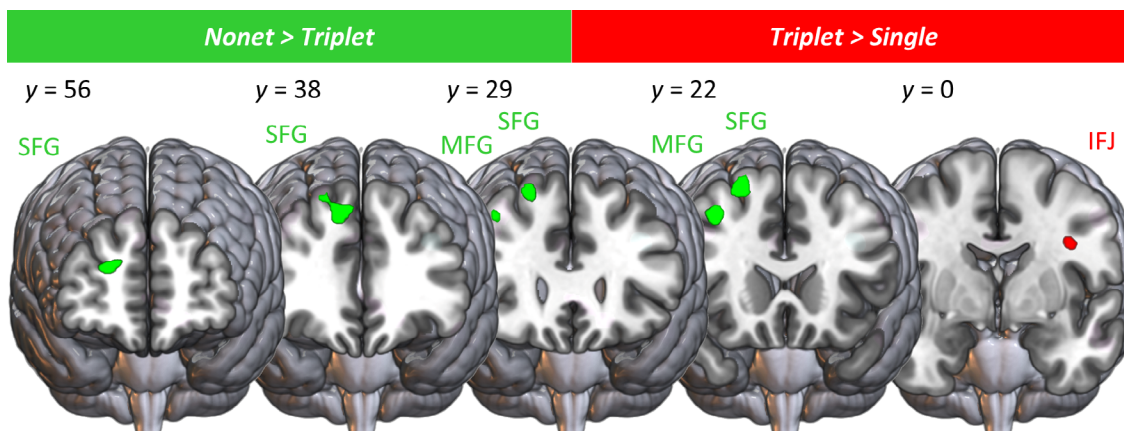


FIGURE 6 BOLD activation clusters in the frontal cortex for the contrasts Triplet > Single and Nonet > Triplet. Significant clusters at the cluster threshold of 47 voxels, depicted on MNI template. BOLD, blood-oxygen-level-dependent; IFJ, Inferior frontal junction; MFG, Middle frontal gyrus; MNI, Montreal Neurological Institute; SFG, Superior frontal gyrus; y, y coordinate.

Nonet-specific beta values are higher in anterior and medial areas, while Triplet specific betas are higher in lateral and more posterior portions of the frontal lobe.

3.3 | RC results

The final set of RC hubs identified with the lausanne120 parcellation (Figure 7c,d) and the group-based connectivity matrix based on 60% prevalence (de Reus & van den Heuvel, 2013a; Figure 7a,b) are depicted in Figure 6. The RC hubs of the remaining identification

methods and a summary of all hub measures can be found in the supplemental material (Figures S5.1 and S5.3 and Tables S6.5–S6.8). The comparison with the HCP-based RC definition is also described in the supplemental material (Table S9.1).

3.4 | ROI analysis results—The function of different structural nodes

The ROI analysis model (Equation 4) tested the influence of HIERARCHY and the NODE CLASSIFICATION (Local, Feeder, RC) as well as their

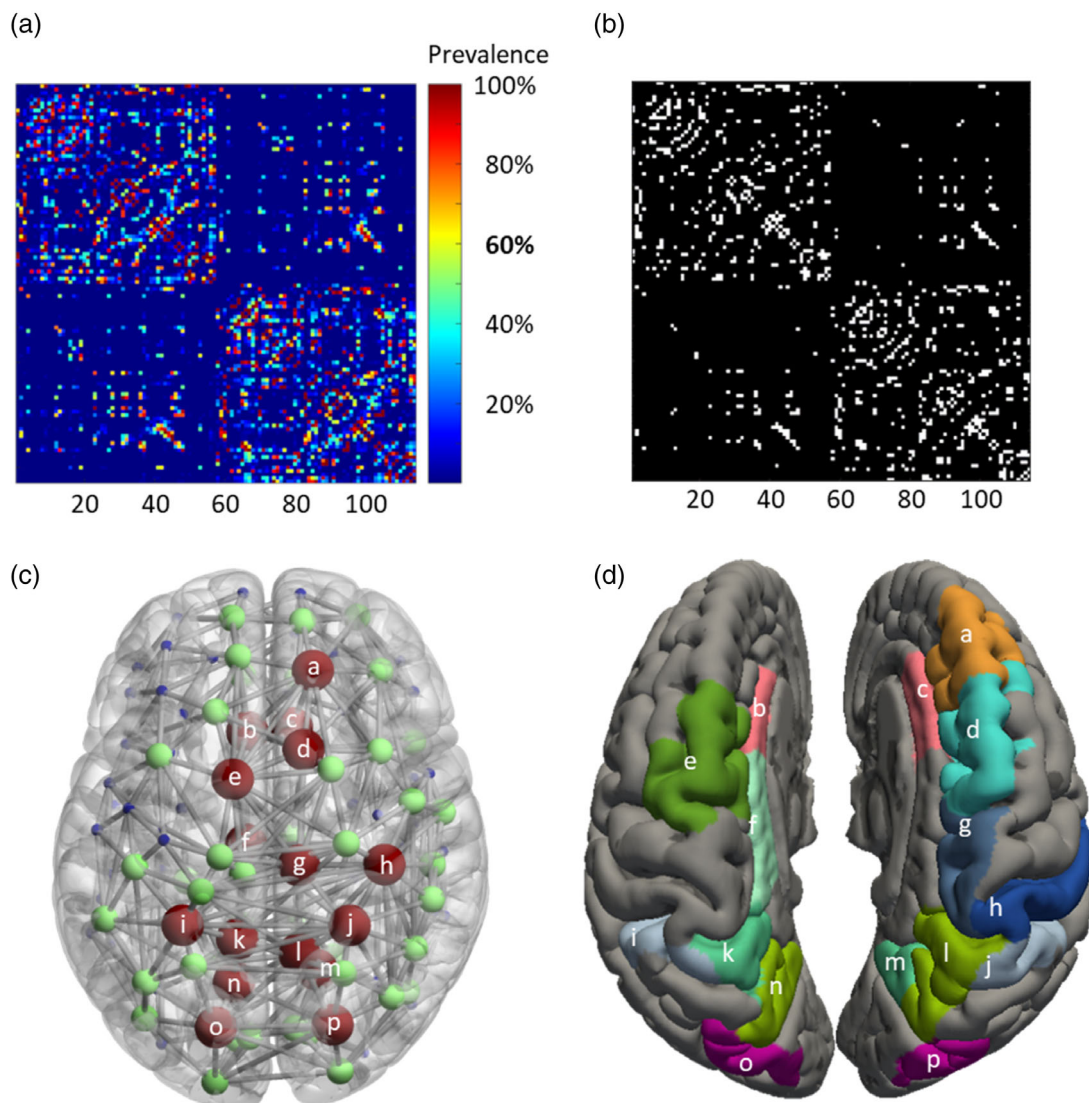


FIGURE 7 Connectivity matrices and rich club network combining lausanne120 parcellation scheme and 60% prevalence-based group matrix. (a) Group matrix depicting prevalence of connection in percent. For further analyses, the matrix was binarized by thresholding at 60% prevalence (Figure 3). (b) Binarized group network based on 60% prevalence threshold. (c) Node classification and identified RC network for the lausanne120 parcellation scheme and a 60% prevalence-based group matrix. Red, RC nodes; green, Feeder nodes; Blue, Local nodes. (d) Surface render of the RC hubs; colors code different parcels of the lausanne120 atlas (lausanne120 labels: (a) right superiorfrontal_2, (b) left caudalanteriorcingulate_1, (c) right caudalanteriorcingulate_1, (d) right superiorfrontal_3, (e) left superiorfrontal_4, (f) left posteriorcingulate_1, (g) right paracentral_1, (h) right postcentral_2, (i) left superiorparietal_1, (j) right superiorparietal_1, (k) left precuneus_1, (l) right precuneus_2, (m) right precuneus_1, (n) left precuneus_2, (o) left superiorparietal_3, and (p) right superiorparietal_3).

interaction on the beta values extracted from the ROIs. We calculated the same model for both group matrix methods (prevalence and *t* test, see Supplemental Material for lausanne250). All beta values were derived from a GLM that estimated the mean activations per condition compared to the implicit baseline. The models differed in the classification of the nodes, corresponding to different group networks (Figures 7c and S5.3). None of the models had divergent transitions and all *R*_{hat} < 1.05. The bulk- and tail-effective samples of each model are given in Table 3 and S4.1–S4.3, respectively. Posterior checks showed that the cumulative count model simulations reasonably capture the means and distributions of the observed data (Figures S7.3–

S7.6). We were especially interested in the interaction of HIERARCHY and NODE CLASSIFICATION. Since the tendencies were the same for both approaches, Table 3 reports the results for the variant lausanne120 parcellation and 60% prevalence-based group matrix (see Tables S4.1–S4.3 for remaining results).

Regarding the expected interaction, we found an increase in the beta values between the conditions Triplet and Nonet for all levels of NODE CLASSIFICATION, and this increase showed a nonsignificant tendency to be stronger for RC hubs and Feeder nodes than for Local nodes. In general, the beta values decreased for the RC hubs and Feeder nodes compared to local nodes (Figure 8 for lausanne120

TABLE 3 Results of the hypothesis test of model Equation 4 for the data from parcellation scheme lausanne120 and 60% prevalence-based group matrix.

Hypothesis	<i>M</i>	<i>SD</i>	CI lower	CI upper	Evidence ratio (BF)	Posterior probability
<i>Increase of beta values with level of Hierarchy separated by node classification</i>						
<i>Local</i>						
Triplet > Single	−0.08	0.12	−0.28	0.12	0.34	0.26
Nonet > Triplet	0.38	0.20	0.06	0.71	33.97	0.97
Complete > Nonet	−0.07	0.16	−0.33	0.19	0.50	0.33
<i>Feeder</i>						
Triplet > Single	−0.04	0.13	−0.25	0.16	0.60	0.37
Nonet > Triplet	0.48	0.20	0.15	0.80	106.91	0.99
Complete > Nonet	−0.12	0.16	−0.38	0.15	0.30	0.23
<i>RC</i>						
Triplet > Single	0.02	0.14	−0.21	0.26	1.33	0.57
Nonet > Triplet	0.43	0.21	0.09	0.77	48.10	0.98
Complete > Nonet	−0.14	0.17	−0.42	0.14	0.26	0.21
<i>Increase of beta values with level of Hierarchy compared between node classifications</i>						
<i>Triplet > Single</i>						
Feeder > Local	0.04	0.07	−0.07	0.15	2.63	0.72
RC > Local	0.10	0.09	−0.04	0.25	7.17	0.88
RC > Feeder	0.06	0.09	−0.09	0.22	3.08	0.76
<i>Nonet > Triplet</i>						
Feeder > Local	0.09	0.07	−0.01	0.20	12.25	0.92
RC > Local	0.05	0.09	−0.10	0.20	2.32	0.70
RC > Feeder	−0.05	0.09	−0.20	0.11	0.44	0.31
<i>Complete > Nonet</i>						
Feeder > Local	−0.05	0.07	−0.16	0.06	0.30	0.23
RC > Local	−0.07	0.09	−0.22	0.08	0.27	0.21
RC > Feeder	−0.02	0.10	−0.18	0.13	0.67	0.40
<i>No difference of beta values between node classifications</i>						
Local = Feeder	−1.04	0.28	−1.59	−0.48	0.01	0.01
Local = RC	−1.39	0.39	−2.14	−0.63	0.04	0.03
Feeder = RC	−0.35	0.4	−1.14	0.47	11.57	0.92

Note: The evidence ratio of one-sided hypothesis tests is equal to the Bayes factor. All *R*_{hat} = 1.00, Bulk_ESS ≥ 3634, Tail_ESS ≥ 5167, *N* = 17,905. Bold values: Evidence ratio/Bayes factor of > 3 (see Section 2.8.6 for more detail) or more precisely from a posterior probability > 0.95. The posterior probability can be interpreted similar to a *p*-value in frequentist statistics. For results in favor of the tested hypothesis the posterior probability must be > 0.95 and for results in favor of the alternative hypothesis posterior probability must be < 0.05. So significance is already given and highlighted. I am not sure, what might be missing.

Abbreviations: BF, Bayes factor; CI, credible interval; RC, rich club.

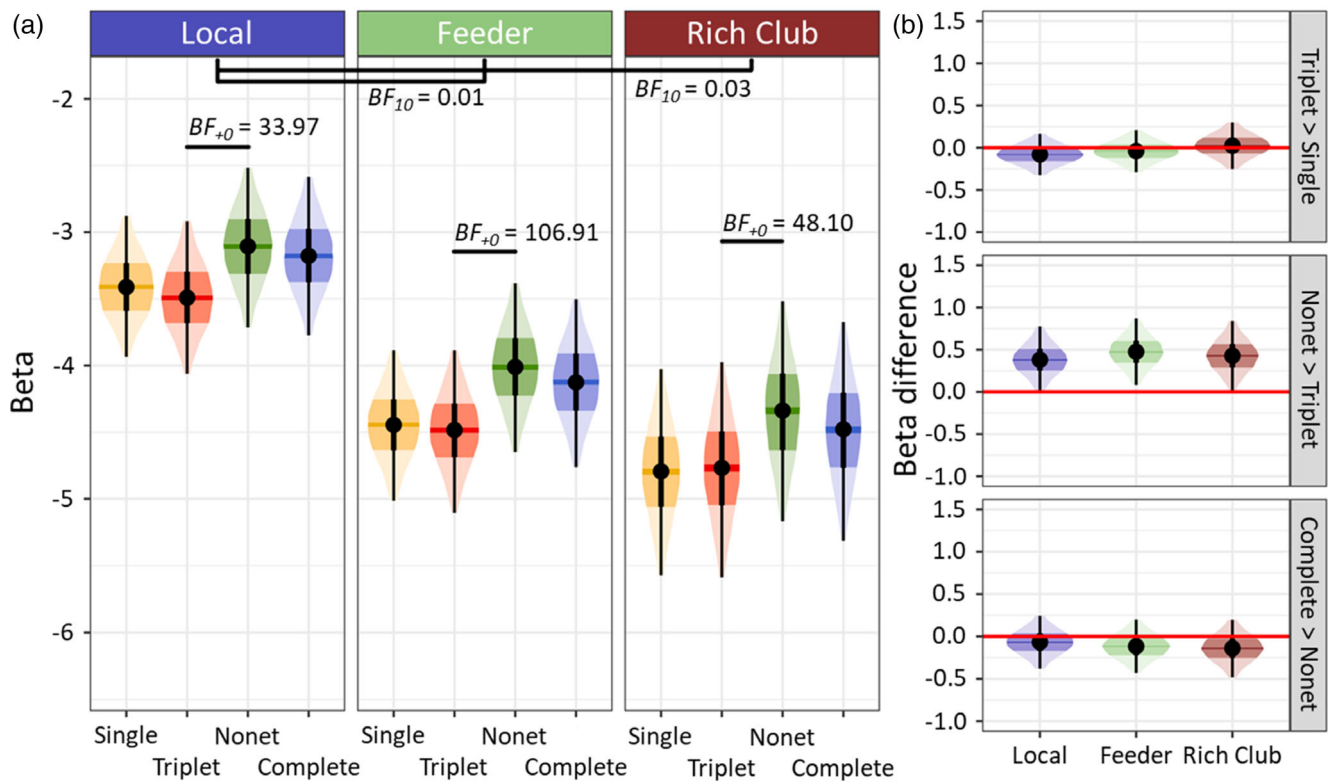


FIGURE 8 Results of region of interest analysis based on lausanne120 parcellation scheme and 60% prevalence-based group matrix. Beta values represent mean activations per condition compared to the implicit baseline. Density plots of posterior distributions with mean point estimate, 50 and 95% highest probability density areas marked. Local, no connection rich club; Feeder, connection to rich club; rich club, rich club hubs. Yellow, Single; Red, Triplet; Green, Nonet; Blue, Complete; Dark blue, Local; Light green, Feeder, Dark red, Rich Club. (A) Level of HIERARCHY estimates in different NODE CLASSIFICATIONS. (B) HIERARCHY differences in different NODE CLASSIFICATIONS. Red line marks no difference.

parcellation and 60% prevalence-based group matrix, Supplemental Material for remaining results).

3.5 | Centrality analysis results—Network centrality of the functional clusters

On a descriptive level, we looked at the regions that were covered by the functional clusters identified in the whole brain analysis (see Section 3.2). Specifically, we examined if the clusters were classified as RC hub, Feeder or Local node and focused on the differences in classification between the Triplet- and Nonet-specific clusters (Figure 9, Supplemental Material for remaining results).

On the model side, we used a MANOVA-like approach within the brms (Bürkner, 2017) framework to compare the centrality measures calculated for each subject between the identified clusters. No model had any divergent transitions, all $Rhat = 1.00$, and all variables had bulk- and tail-effective samples ≥ 4173 and ≥ 4061 , respectively. Posterior checks showed that the cumulative count model simulations reasonably capture the means and distributions of the observed data (Figure S7.7).

First, we compared the model (Equation 5) including the factor HIERARCHY CONTRAST with a null model, to see if the factor explained

any variance of the centrality measures. The leave-one-out-cross-validation (loo) comparison revealed a significant increase in the expected log pointwise predictive density (elpd) with the inclusion of the factor HIERARCHY CONTRAST (Table 4).

Next, we specifically tested whether the centrality measures of the areas derived from the Nonet > Triplet contrast were higher than those for the Triplet > Single contrast. Only the within-module degree z-score, which describes the module-specific degree of a node (Rubinov & Sporns, 2010), failed to show the predicted effect. For degree centrality, closeness centrality, betweenness centrality, and the participation coefficient the Nonet > Triplet clusters demonstrated the expected effect displaying significantly higher scores (Table 5 and Figure 10). This pattern shows that functional activation clusters for hierarchically higher structures of the stimulus coincide with areas of higher structural network centrality.

4 | DISCUSSION

Humans show a preference for exploring higher-order structures in the presence of complex, hierarchically nested, eventful stimuli such as actions (Williams et al., 2022) or language (Yedetore et al., 2023). In the current study, we used DWI and fMRI to investigate the

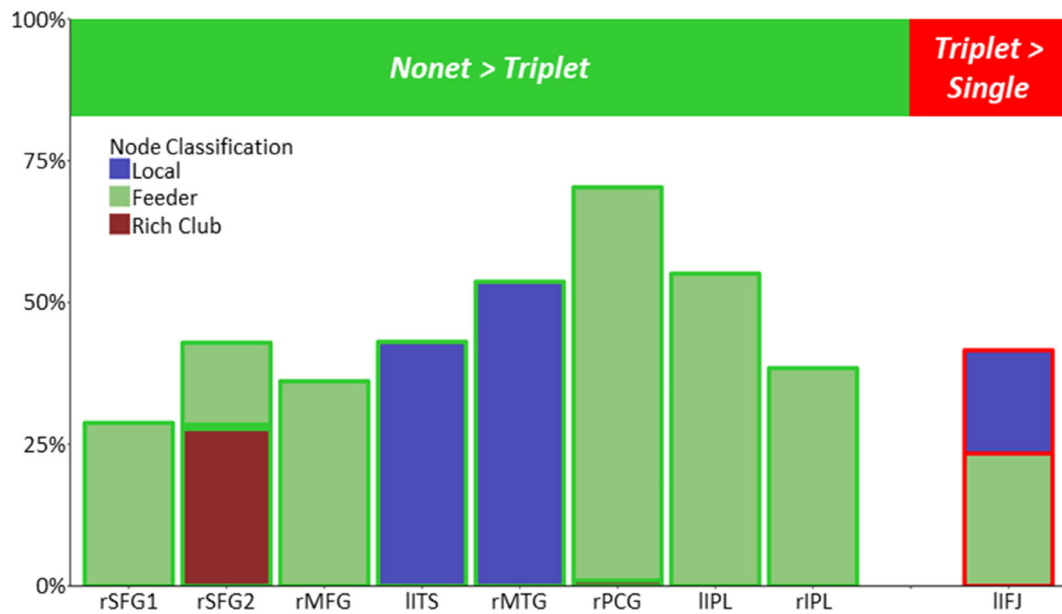


FIGURE 9 Percentage of overlap of activation clusters of the whole brain analysis with the parcellation. Colored according to lausanne120 and 60% prevalence-based NODE CLASSIFICATION. IFJ, inferior frontal junction; IPL, inferior parietal lobule; ITS, inferior temporal sulcus; l, left; MFG, middle frontal gyrus; MTG, middle temporal sulcus; PCG, posterior cingulate gyrus; r, right; rSFG1, rSFG (22, 60, 14); rSFG2, rSFG (22, 18, 58); SFG, superior frontal gyrus.

Model	\widehat{elpd}_{diff}	$se(\widehat{elpd}_{diff})$	\widehat{elpd}_{loo}	$se(\widehat{elpd}_{loo})$
Hierarchy contrast + (1 Subject)	0.0	0.0	-1817.70	42.36
1 + (1 Subject)	-12.7	3.6	-1830.40	42.19

TABLE 4 Fit indices of the HIERARCHY contrast model (Equation 5) compared to the null model for lausanne120 parcellation scheme.

Note: Models are considered to be better if the absolute difference is larger than the standard error (Mohor et al., 2021); \widehat{elpd}_{loo} , expected log pointwise predictive density for a new dataset using PSIS leave-one-out-cross-validation (loo) criterion. The closer to zero the better the model; \widehat{elpd}_{diff} , difference between the \widehat{elpd}_{loo} of the two compared models; se , standard error of the variable. Abbreviation: PSIS, Pareto smoothed importance sampling.

TABLE 5 Results of testing (Nonet > Triplet) > (Triplet > Single) for model Equation 5 for all five centrality measures extracted from individual connectivity matrices following lasusanne120 parcellation scheme.

Centrality measure	M	SD	CI lower	CI upper	Evidence ratio (BF)	Posterior probability
Degree centrality	0.59	0.16	0.32	0.85	>999	1
Closeness centrality	0.28	0.16	0.02	0.54	26.73	0.96
Betweenness centrality	0.54	0.16	0.27	0.81	>999	1
Within-module degree z-score	-0.21	0.17	-0.49	0.06	0.12	0.10
Participation coefficient	0.46	0.17	0.19	0.73	>999	1

Note: The evidence ratio of one-sided hypothesis tests is equal to the Bayes factor. Abbreviations: BF, CI, credible interval; RC, rich club.

importance of the brain's intrinsic hierarchical structure for processing nested hierarchical stimuli. To identify brain structures that process hierarchically higher stimulus structures, we presented subjects with different levels of hierarchically nested digit sequences. We collected DWI data from the same participants to determine the global hierarchical node structure of the brain expressed in Local and,

Feeder nodes, and RC hubs. We tested two separate hypotheses: (I) We hypothesized that the processing of hierarchically higher stimulus structures would involve network hubs that are part of the RC. (II) We also expected a trend toward more anterior and medial regions of the frontal cortex for processing hierarchically higher stimulus structures.

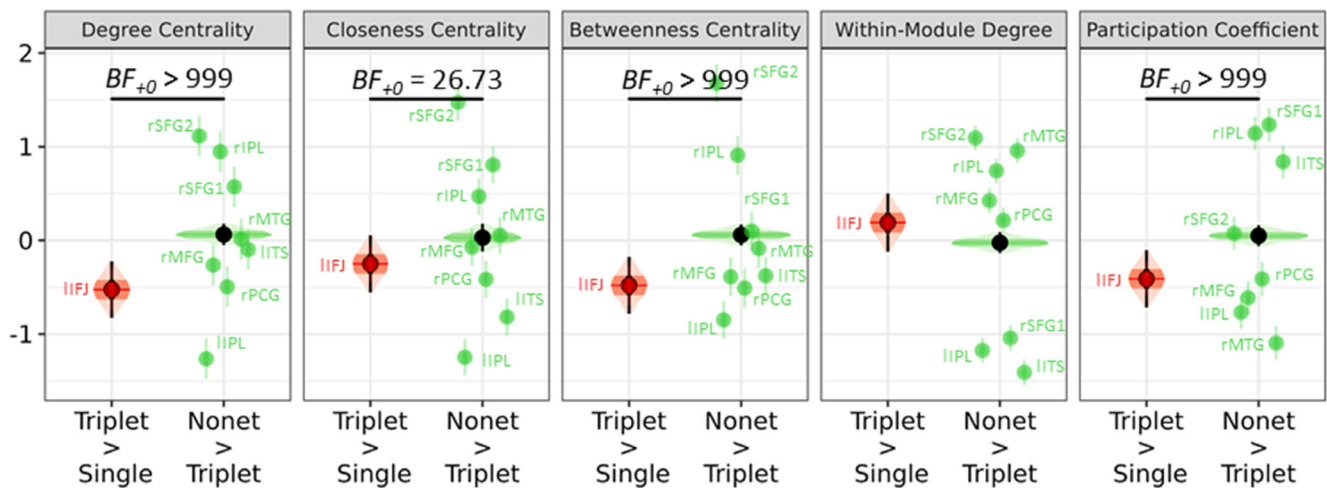


FIGURE 10 Results of the centrality analysis for lausanne120 parcellation scheme. Density distributions with mean point estimate, 50 and 95% highest probability density areas marked. Centrality measures are controlled for cluster size and z-standardized for comparability. Eye plots describe distribution of contrast on average, colorful point-interval plots describe each individual cluster. BF, Bayes factor; IFJ, inferior frontal junction; IPL, inferior parietal lobule; ITS, inferior temporal sulcus; l, left; MFG, middle frontal gyrus; MTG, middle temporal sulcus; PCG, posterior cingulate gyrus; r, right; rSFG1, rSFG (22, 60, 14); rSFG2, rSFG (22, 18, 58); SFG, superior frontal gyrus.

4.1 | fMRI results—The anterior–posterior and medial–lateral gradient

BOLD activation results confirmed the expected shift toward more anterior and medial regions for processing hierarchically higher structures. Visually inspecting the frontal activation clusters of the step-wise contrasts of the Nonet > Triplet blocks and the Triplet > Single blocks, we can describe the clusters in the Nonet-specific activations were located in more anterior and medial areas of the SFG and MFG. The only Triplet-specific cluster, however, was found in the more posterior and lateral IFJ. Additionally, we examined the correlations between contrast-specific beta values and the distance from the anterior-medial section of the frontal lobe. The comparison between Nonet- and Triplet-specific correlations revealed that the Nonet-specific activations increased closer to the anterior-medial frontal cortex. The Triplet-specific beta values in contrast significantly increased with distance. Thus, the correlations provide evidence for the anterior-medial shift for processing hierarchically higher stimulus structures beyond the visual inspection of the identified clusters.

The concept of a posterior-to-anterior processing gradient throughout the frontal lobe has been discussed even before the dawn of brain imaging (Ingvar, 1985). This gradient was proposed to be organized according to the temporal persistency of the processed levels (Fuster, 2001; Golesorkhi, Gomez-Pilar, Zilio, et al., 2021; Kiebel et al., 2008; Koehlin & Summerfield, 2007; Uithol et al., 2012). Also, it was found not only in fMRI BOLD responses (Badre & D'Esposito, 2007; Koehlin et al., 1999) but also in cytoarchitecture (Chanes & Feldman Barrett, 2016; Hilgetag et al., 2016; Sanides, 1964) and recently also in patterns of cortical frequencies (Mahjoory et al., 2020; Raut et al., 2020). Notably, this progression of time scales might also characterize the association cortices in the parietal and temporal lobes as well, which were found to integrate

information across time (Badre & Wagner, 2004; Bussey & Saksida, 2005; Cui, 2014; Golesorkhi, Gomez-Pilar, Zilio, et al., 2021; Jeon, 2014; Kravitz et al., 2013; Naya et al., 2003). Yet, theoretical and empirical work sees the frontal lobe at the top of the entire cortical processing hierarchy (Brunia, 1999; Fuster & Bressler, 2015; Gómez et al., 2004; Koehlin et al., 1999; E. K. Miller & Cohen, 2001). However, the initial notion of the frontal pole being the apex of the hierarchy has been challenged by several findings (Badre & Nee, 2018; Crittenden & Duncan, 2014; Goulas et al., 2014; Nee & D'Esposito, 2016; Ramnani & Owen, 2004; Reynolds et al., 2012). More recent studies included the structure of cortical layers in the gradient and argued for more medial aspects of the PFC and the limbic system to be superordinate to the frontal pole (W. H. Alexander & Brown, 2018; Chanes & Feldman Barrett, 2016; Nee & D'Esposito, 2016). This progression from posterior-lateral toward anterior-medial frontal lobes for processing hierarchically higher structures of stimuli was also reflected in our results (Figure 6, also Supplemental Material).

Beyond the frontal effects our hypotheses focused on, the Nonet > Triplet contrast also revealed significant activation clusters in posterior parietal cortex. The lateral fronto-parietal network has been related to the processing of numbers (Dormal et al., 2012; Goffin, 2019; Sokolowski et al., 2017) and numerical magnitude (Ansari et al., 2006; Molko et al., 2003; Piazza et al., 2004, 2007), including the so-called mental number line in the angular gyrus (Dehaene et al., 2003). More generally, the parietal cortex is proposed to provide frontal areas with information about spatial and temporal relational metrics such as order, number, duration, length, distance, and proportion (Genovesio et al., 2014). Because digits were presented and processed in all conditions in our study, one might suggest that the hierarchically higher structure of the digit sequences (Nonet > Triplet) required greater temporally extended integration that is also associated

with the fronto-parietal network (Bor & Seth, 2012; Golde et al., 2010; Hasson et al., 2015; Noonan et al., 2013).

4.2 | RC analysis—A largely consistent structure emerges

Based on the DWI data, we identified the structural graph including Local, Feeder, and RC areas, for the RC analysis. The RC hubs we identified closely resemble those hub regions identified by previous studies, including those in the bilateral precuneus and bilateral superior parietal lobe (Q. Cao et al., 2013; Z. Chen et al., 2013; Hagmann et al., 2010; Riedel et al., 2022; Wang, Zhan, et al., 2019), in the bilateral superior frontal gyri (Q. Cao et al., 2013; Z. Chen et al., 2013; Riedel et al., 2022; Wang, Zhan, et al., 2019), the anterior and posterior cortex cingulate (Huang et al., 2015) as well as the paracentral lobe (Z. Chen et al., 2013) and the superior and middle occipital lobe (Q. Cao et al., 2013; Z. Chen et al., 2013; Huang et al., 2015).

Although the results of network measures are sufficiently reliable even with the use of different methods, there is still no gold standard for identifying RC hubs or graph-theoretical measures in general (Braun et al., 2012; H. Cao et al., 2014; Welton et al., 2015). Most studies use only nodal degree-relative thresholds to determine RCs (Keown et al., 2017; O'Donoghue et al., 2017; Ray et al., 2014; van den Heuvel et al., 2013; Yan et al., 2018). In contrast, we decided to implement additional criteria for a node to qualify as an RC hub. In particular, we followed the definition of Colizza et al. according to which RC hubs are more densely connected to other high-degree nodes than expected in a random network (Colizza et al., 2006). As far as we can see, we are the first to apply this additional, theory-based step in the identification process, although as early as van den Heuvel and Sporns (2013) it was recommended to use more than just the degree as an identifier for the RC membership. A degree-based definition of hubs may generally be inadequate for identifying network structures that are important for global network communication. For instance, structures characterized by specific nodal properties such as an exceptionally high participation coefficient, making up a *diverse club*, might be more critical for efficient global integration than the RC hubs' outstanding connection strength (Bertolero et al., 2017).

However, as a result of using not just the degree to identify hubs, we did not find all RC hubs that are typically reported when more liberal criteria are applied. For instance, while we identified the insula as a highly connected node when following the criteria for RC qualification introduced by Riedel et al. (2022), this node failed to be more connected to other high-degree nodes than expected at random (Tables S6.1–S6.4). The insula, though commonly reported as a hub (Q. Cao et al., 2013; Z. Chen et al., 2013; Riedel et al., 2022), was even labeled as a Local node, according to our definition, as it was not directly connecting to any other RC hub. Especially because of these discrepancies between our results using additional constraints in the RC hub identification and the hubs found in the related literature, the performed validation analysis using the HCP data was a crucial step. According to the conventions for inter-rater reliability by Landis and

Koch (1977), the results showed only a slight agreement (Table S9.1) in hub identification. Thus, sticking with the insula as an example, the parcels of the insula in the HCP dataset were mostly identified as Feeder nodes. Occasionally across the different parcellation schemes and group matrix creation methods some insula parcels were even classified as RC hubs. But importantly, areas that were found to be crucial for the processing of hierarchically higher stimulus structures (J. Chen et al., 2017; Hasson et al., 2015) and were consistently found as RC hubs in previous studies (e.g., Riedel et al., 2022) like parcels in the superior frontal cortex or the precuneus were identified in both our own and the HCP dataset (Tables S6.1–S6.4 and Table S9.8). Thus, the consistent findings between both datasets for the ROI and centrality analyses might be especially influenced by these coherently identified RC hubs.

To summarize, the applied RC hub identification in this article adheres more closely to the original definition of the RC by Colizza et al. (2006). Therefore, the identified hubs can be more likely considered as RC hubs, while other identification methods that, for example, only use the node degree might rather identify general hubs, not necessarily RC hubs. Nevertheless, this method is still dependent on acquisition parameters and processing of the connectivity matrices (some decision will be discussed in Section 4.4). Hence, more research is necessary to determine if the proposed extra step of comparing the hub connections to the connectivity in random networks is a valuable improvement to the RC identification methodology.

4.3 | Combining the results—The significance of RC hubs for the processing of nested hierarchical stimuli

To our knowledge, our study was the first to attempt to relate task-based fMRI activity to the structurally determined RC in the same group of subjects. Therefore, we developed the described procedures specifically for this analysis. We applied two complementary approaches, the ROI analysis, and the centrality analysis, to tackle the question of the functional significance of the structural hubs from different sides, which will be discussed separately in the following paragraphs. As mentioned before, these methods of combining structure and function both prevent any notion of circularity by identifying their areas of interest and outcome variables drawn from them crossmodally based on the fMRI and structural connectivity data, respectively (Kriegeskorte et al., 2009).

On the one hand, we modeled the beta values extracted from each parcel by their condition (HIERARCHY) and network relevance (NODE CLASSIFICATION). Especially looking at the activations within the RC hubs, Feeder nodes, and Local nodes revealed that all three kinds of nodes were depicting the same pattern of activity: Beta values were higher for the Nonet condition in comparison to the Triplet condition, while the Single and Triplet conditions as well as the Nonet and Complete did not differ significantly. Using the node classifications from the HCP validation dataset we were able to replicate the same pattern (Figure S9.1 and Tables S9.2–S9.5). We found a

nonsignificant trend that the Nonet > Triplet difference was slightly larger for RC and Feeder nodes than for Local nodes. When using the HCP dataset-based classification of nodes and the *t* test-based group matrices the difference between the Nonet and Triplet was significantly larger in RC hubs for both parcellation schemes (Tables S9.3 and S9.5 and Figures S9.1B and S9.1D).

Nevertheless, due to the inconsistent results, the hypothesis that RC hubs are specifically more involved in the processing of hierarchically higher structures of stimuli could neither be confirmed nor disproven with our analysis. However, this very similar activation pattern in Local, Feeder, and RC nodes could be a direct result of a core function of the RC, namely network synchronization (Gómez-Gardeñes et al., 2010; Senden et al., 2017; Watanabe, 2013). Specifically, Gollo et al. (2015) found that the RC hubs sit on top of so-called resonant network motifs, each consisting of three non-fully connected nodes with edges facing away from the central node. These network motifs are particularly efficient at synchronizing the activity of their neighboring nodes. Thus, finding very similar activation patterns all across the brain regardless of the type of node might indicate that the activation is synchronized throughout the network. The well-connected RC could be the prime candidate to achieve this synchronization. In order to assess the influence of the RC on the overall neural network, other methods may be more informative than those that average neural activity over the entire time span of the experiment. The synchronization effect imposed by the RC can be tested using the autocorrelation of the network nodes (Aguilar-Velázquez & Guzmán-Vargas, 2019). For instance, the autocorrelation decay method was recently used to show different intrinsic timescales across the cortex (Ito et al., 2020; Raut et al., 2020). Using this approach could reveal additional information on the dynamic influence of the RC hubs on the rest of the network and its modulation depending on the task at hand.

On the other hand, we analyzed the centrality measures obtained from the structural nodes at the location of significant functional clusters to assess the cluster's network importance. To this end, we first inspected the network-based classification of each of the functionally identified clusters. As a result, the clusters in the frontal and parietal lobes and the PCG cluster were contained in parcels that were classified as RC hubs or Feeder nodes. In contrast, the temporal lobe activity identified in the Nonet > Triplet contrast belonged to parcels that were classified as Local nodes. Also, the cluster in the left IFJ identified in the Triplet > Single contrast did not overlap with any parcels that were labeled as RC hubs. While a little less distinct, using the node classification from the HCP dataset, we could again show a tendency of the Nonet-specific clusters to share more overlap with parcels that were classified as RC hub (see Supplemental Material). So, compared with Triplet-specific activation cluster, Nonet-specific clusters showed greater overlap with the locations of RC hubs and Feeder nodes in frontal and parietal cortices. This observation is consistent with the hypothesis that hierarchically higher stimulus structures were processed in, or closer to, the structurally identified RC hubs.

Based on this overlap between the functionally found clusters and the network nodes, we extracted the following five centrality measures from the structural network nodes underlying the functional

clusters: degree centrality, closeness centrality, betweenness centrality, within-module degree z-score, and participation coefficient. We expected that the centrality measures of nodes underlying the Nonet-specific clusters would be higher than for the Triplet-specific cluster. We indeed found a general significant influence of the HIERARCHY CONTRAST, an effect depending on whether the cluster was Nonet- or Triplet-specific, on the examined centrality measures. This general effect was replicated also using structural centrality measures extracted from the HCP data. Looking at the individual measures, the predicted effect was identified for degree centrality, betweenness centrality and the participation coefficient for both parcellation schemes and additionally for closeness centrality using the lausanne120 parcellation. Similarly, the individual measures from the HCP data also differed significantly between the Nonet-specific and Triplet-specific clusters extracted from functional data presented in this article. Significant differences were found for degree centrality and participation coefficient for both parcellation schemes, and additionally for betweenness centrality for the lausanne120 parcellation (Table S9.7 and Figure S9.3). Thus, the results of the centrality analysis largely met our expectations and were also very similar across the two parcellation schemes and datasets. The found differences for degree centrality, betweenness centrality and closeness centrality suggest that the structural nodes underlying Nonet-specific activations are more important for the integration and resilience of the connectome than the Triplet-specific cluster (Rubinov & Sporns, 2010). The consistent finding of an increased participation coefficient for Nonet-specific clusters further indicates that these nodes are also more structurally connected to different modules. The participation coefficient is usually interpreted and investigated alongside the within-module degree z-score (e.g., Fukushima et al., 2018; Jao et al., 2020; Pedersen et al., 2020). Only nodes with a high within-module degree and high participation coefficient are described connector nodes, which encourage global integration (Guimerà & Nunes Amaral, 2005; Rubinov & Sporns, 2010) and are crucial for communication across the cortical network (Crossley et al., 2014; Wu et al., 2011). Yet, the previously mentioned diverse club is just characterized by high participation coefficient nodes and their connectivity (Bertolero et al., 2017) showing that nodes with a high participation coefficient alone could indicate importance for the network's communication. More research on centrality measures is necessary to settle if there are meaningful and systematic relations between individual graph centrality measures of nodes and their function. This could be especially intriguing as the dynamic association between structural and functional networks was found to be dependent on the segregation or integration of the functional network (Fukushima et al., 2018).

In summary, the results of the centrality analysis demonstrate that areas that are functionally activated by hierarchically higher stimulus structures are more important for the integration and integrity of the structural network. In combination with the larger overlap of these functional clusters with RC hub regions, these results provide potential evidence for the hypothesis that the RC hubs are more involved in the processing of hierarchically higher structures of incoming stimuli.

Taken together, both the ROI and centrality analysis allude to the involvement of RC hubs in the processing of hierarchically higher stimulus structures. In this context, it has to be pointed out that the results were very consistent across methods of parcellation and group-matrix creation and were even replicated using a large independent structural dataset. Thus, even though, the methods for combining structure and function in this article were specifically developed for the investigated question and consequently applied for the first time, the displayed consistency of the found results demonstrates their suitability.

4.4 | Limitations and open questions

Some limitations of the study have to be considered. The paradigm and stimulus structure we applied was based on the TRW approach (Hasson et al., 2008, 2010). As previous findings using this approach could demonstrate a distinction of specific areas activated for certain hierarchical structures in the stimulus levels and that the additionally engaged areas per hierarchical level also extend along an anterior-posterior gradient (Farbood et al., 2015; Lerner et al., 2011), we as well expected to find a distinction between the four levels implemented in our stimulus sequences. However, neither the behavioral, neurofunctional, nor ROI analysis results could consistently distinguish between the four implied hierarchical levels. The ROI results rather showed a distinction between a hierarchically low (Single and Triplet) and hierarchically high (Nonet and Complete) level. Especially the Complete condition behaved unexpectedly across all analyses, as it did not differ from the Nonet condition in any applied contrast. It can be speculated that the 36-digit sequence of the Complete condition was too long for subjects to notice the repeating pattern of digits. If the stimuli are processed one by one as they are presented, studies on working memory capacity would predict a maximum capacity of nine items depending on the modality (Bick & Rabinovich, 2009; G. A. Miller, 1956). This would include the ranges for the Single, Triplet, and Nonet conditions and might also explain the similarity of the Nonet and Complete conditions as they are practically the same when only looking at the last nine digits.

A second limitation relates to the method of structural network reconstruction and RC hub identification. In constructing the connectivity matrices used for the RC analysis, we decided on the one hand to binarize the matrices and on the other hand to use group-averaged matrices. The binarization was implemented as a necessary compromise (Calamante, 2019). Since the acquisition parameters of our DWI sequence did not fully comply with current recommendation (Jones et al., 2013), we binarized the structural connectivity matrices to mitigate biases that can occur when using weighted graphs with subpar DW data (Fornito et al., 2016). The decision to use a group-wise connectivity matrix was made because we employed group-level statistics for the combination of functional and structural data. Additionally, it has been already shown that large structural connectivity patterns, such as the RC, are more detectable in group-connectomes (Hagmann et al., 2008). Still, it should be considered that both steps

reduce the information included in the analysis, which affects the interpretability and generalizability of the results (Calamante, 2019). However, the consistency of results across parcellation schemes, group matrix creation methods and datasets demonstrated in this article nonetheless supports the credibility of our findings.

Furthermore, for the parcellation schemes, we opted for the extensions of the FreeSurfer inherent Desikan-Killiany atlas introduced in Cammoun et al. (2012) that are included in CATO (de Lange et al., 2023). More precisely, we used the lausanne120 and lausanne250 options with 114 and 219 cortical areas, respectively, as this resolution might come closer to meso-level parcellations related to multimodal differences between the areas (Amunts & Zilles, 2015). However, while the Desikan-Killiany atlas is based on the borders of gyri and sulci (Desikan et al., 2006), thus having an anatomical justification, the extensions aimed for a near voxel-level parcellation and are not particularly based on any natural borders in the cortex (Cammoun et al., 2012). Parcellation on the levels of voxel size is referred to as random (Qi et al., 2015) as the resolution becomes arbitrary (de Reus & van den Heuvel, 2013b). An increase in parcellation resolution would also require an improvement in DWI quality (Yeh et al., 2018). It can, however, be argued that the level of detail of the chosen parcellation might be dependent on the purpose of the investigation, as a “correct” parcellation is unlikely to be accomplished (Schaefer et al., 2018). Nevertheless, in trying to bridge the gap between structural connectivity and cortical function, it might be more interesting to utilize a parcellation scheme that uses functional information as the basis for boundaries (Craddock et al., 2012; Schaefer et al., 2018; Shen et al., 2013), or even an approach using multiple sources of information (Glasser et al., 2016). This is especially relevant since the parcellation scheme has been shown to largely influence the appearance of the network (Bassett et al., 2011; Bryce et al., 2021; Cammoun et al., 2012; Qi et al., 2015; Seguin et al., 2020; Sporns, 2011), which can also be seen in this study when comparing the networks between the lausanne120 and lausanne250 parcellations (Figure S5.3).

Also, we varied the method that constructed the group connectivity matrix. The prevalence method was based on the false-positive and false-negative balance calculation (de Reus & van den Heuvel, 2013a), while the *t* test method was based on the analyses in Ponsoda et al. (2017). Since the results differed especially for the lausanne250 parcellation scheme between the two methods (Figure S5.3), it might be necessary to investigate the false-positive rates, like de Reus and van den Heuvel (2013a) did before, depending on the parcellation scheme used. Previously it could be shown that graph theoretical measures are only more reliable with lower resolution parcellations (Welton et al., 2015) which in turn might be less representative for a functionally viable parcellation of the cortex (Amunts & Zilles, 2015).

Finally, we did not include the subcortex since the focus of the functional analysis was on cortical activations. Hence, our approach was not designed to identify subcortical hubs as others did, for instance in the thalamus, putamen, and caudate nucleus (Riedel et al., 2022). The DTI algorithms used to reconstruct the white matter

streamlines for structural connectivity analyses are less reliable in the subcortex due to kissing and crossing fibers (Prčkovska et al., 2016). Even though, we used a combined DTI and GQI algorithm, which showed good performance in the benchmarking test (de Lange et al., 2023), additional methodical considerations regarding DWI sequence and tract algorithm are necessary to accurately identify the streamlines and model the connectivity of the subcortex (Kai et al., 2022). Nevertheless, via basal ganglia-thalamocortical loops, the subcortical areas play a major role in shaping the cortical hierarchy (G. E. Alexander et al., 1986; Badre & Nee, 2018). Thus, given a reliable acquisition and tract-detection, investigating the relationship between structural connectivity in the subcortex and the processing hierarchically structured stimuli could be a compelling next step. Especially, as the striatum is commonly found as an RC hub (Riedel et al., 2022) and also is a key structure for the chunking of sequences, it could be vital for the processing of nested hierarchical structures (Graybiel, 2008).

This article considered both graph-theoretical and anatomical gradients but did not intend to determine which one is better suited to describe our brain's organization. In fact, either gradient may explain distinct portions of variance (Golesorkhi, Gomez-Pilar, Tumati, et al., 2021). Recent studies on cortical gradients explored methods to combine and compare different gradient definitions (Hansen et al., 2022; Suárez et al., 2020). For instance, approaches using resting-state fMRI could already demonstrate the relationship between the intrinsic timescales and structurally determined measures of centrality (Fallon et al., 2020; Lurie et al., 2023; Sethi et al., 2017) as well as cytoarchitectonic (Gao et al., 2020) and functional unimodal to transmodal gradients (Shafiei et al., 2020; Wolff et al., 2022). Future studies should compare gradients defined by various modalities not only in respect to the brain's resting state but also with regard to their task-relevance.

5 | CONCLUSION

To summarize, we could observe a shift of activation clusters for processing hierarchically higher stimulus structures toward more anterior and medial areas in the frontal cortex. The evidence for the importance of structural RC hubs for processing of hierarchically higher structures in nested stimuli, however, remains inconclusive. On the one hand, we determined a set of hub structures that match previously found compositions of the RC. We also are the first to demonstrate that areas in the frontal and parietal regions of the brain that are related to the processing of hierarchically higher structures of stimuli share more overlap with areas that were identified as RC hubs or directly connected Feeder nodes. Also, these areas identified for the functional processing of higher levels were found to be more central to the structural network. On the other hand, while the ROI analysis did determine the involvement of RC hubs in the processing of hierarchically higher stimulus structures, the found activity pattern was not specific to the RC and was instead found across all node classifications. This alludes to a more complex relationship between the

functional processing of hierarchically structured stimuli and the levels of nodes in the structural network. We suggest alternative analysis methods that focus more on the temporal structure of the neurofunctional signal as well as possible refinements of the hub identification methods to further assess the relationship between the hierarchy of our cortical network and the hierarchical structures in the world around us.

AUTHOR CONTRIBUTIONS

Falko Mecklenbrauck contributed project conceptualization, experimental design and setup, data acquisition and analysis, data interpretation, writing and revising the manuscript. Sophie Siestrup contributed data analysis, writing and revising the manuscript. Marius Gruber and Ima Trempler contributed data analysis and writing the manuscript. Anoushiravan Zahedi contributed supervision of the project, data analysis, data interpretation, and writing the manuscript. Dominik Grotegerd and Marco Mauritz contributed data analysis. Udo Dannlowski contributed resources and writing the manuscript. Ricarda I. Schubotz contributed project conceptualization, experimental design and setup, supervision of the project, data analysis, resources, writing and revising the manuscript.

ACKNOWLEDGMENTS

Data were provided in part by the Human Connectome Project, WU-Minn Consortium (Principal Investigators: David Van Essen and Kamil Ugurbil; 1U54MH091657) funded by the 16 NIH Institutes and Centers that support the NIH Blueprint for Neuroscience Research; and by the McDonnell Center for Systems Neuroscience at Washington University. The authors thank Monika Mertens and Lena M. Puder for their help during data collection; Lena M. Puder, Simon Wieczorek, and Maria L. Hofmann for help in the quality control process; Kristin Stroop and Simon Wieczorek for help in testing the paradigm; Alea M. Bexten and Leon G. Exeler for their help in extracting the regions of interest maps; and Maria L. Hofmann and Juliane Diefenthal for their help in revising the manuscript. Open Access funding enabled and organized by Projekt DEAL.

FUNDING INFORMATION

The authors received no specific funding for this work.

CONFLICT OF INTEREST STATEMENT

The authors have declared that no competing interests exist.

DATA AVAILABILITY STATEMENT

The data that support the findings of this study are available from the corresponding author (Falko Mecklenbrauck, f_meck01@uni-muenster.de) upon request. The authors can confirm that all relevant data are included in the article.

ORCID

Falko Mecklenbrauck  <https://orcid.org/0000-0002-8187-6826>

Marius Gruber  <https://orcid.org/0000-0002-6094-9950>

Sophie Siestrup  <https://orcid.org/0000-0002-6365-3055>

Anoushiravan Zahedi  <https://orcid.org/0000-0002-5532-3910>
 Dominik Grotegerd  <https://orcid.org/0000-0001-8718-0128>
 Ima Trempler  <https://orcid.org/0000-0003-2968-4795>
 Udo Dannlowski  <https://orcid.org/0000-0002-0623-3759>
 Ricarda I. Schubotz  <https://orcid.org/0000-0001-5802-6869>

REFERENCES

- Agcaoglu, O., Wilson, T. W., Wang, Y. P., Stephen, J., & Calhoun, V. D. (2019). Resting state connectivity differences in eyes open versus eyes closed conditions. *Human Brain Mapping*, 40(8), 2488–2498. <https://doi.org/10.1002/hbm.24539>
- Aguiar-Velázquez, D., & Guzmán-Vargas, L. (2019). Critical synchronization and 1/f noise in inhibitory/excitatory rich-club neural networks. *Scientific Reports*, 9(1), 1–13. <https://doi.org/10.1038/s41598-018-37920-w>
- Aguirre, G. K., Mattar, M. G., & Magis-Weinberg, L. (2011). De Buijn cycles for neural decoding. *NeuroImage*, 56(3), 1293–1300. <https://doi.org/10.1016/j.neuroimage.2011.02.005>
- Alexander, G. E., DeLong, M. R., & Strick, P. L. (1986). Parallel organization of functionally segregated circuits linking basal ganglia and cortex. *Annual Review of Neuroscience*, 9, 357–381. <https://doi.org/10.1146/annurev.ne.09.030186.002041>
- Alexander, W. H., & Brown, J. W. (2018). Frontal cortex function as derived from hierarchical predictive coding. *Scientific Reports*, 8(1), 1–11. <https://doi.org/10.1038/s41598-018-21407-9>
- Amunts, K., & Zilles, K. (2015). Architectonic mapping of the human brain beyond Brodmann. *Neuron*, 88(6), 1086–1107. <https://doi.org/10.1016/j.neuron.2015.12.001>
- Andersson, J. L. R., Skare, S., & Ashburner, J. (2003). How to correct susceptibility distortions in spin-echo echo-planar images: Application to diffusion tensor imaging. *NeuroImage*, 20(2), 870–888. [https://doi.org/10.1016/S1053-8119\(03\)00336-7](https://doi.org/10.1016/S1053-8119(03)00336-7)
- Andersson, J. L. R., & Sotiropoulos, S. N. (2016). An integrated approach to correction for off-resonance effects and subject movement in diffusion MR imaging. *NeuroImage*, 125, 1063–1078. <https://doi.org/10.1016/j.neuroimage.2015.10.019>
- Ansari, D., Dhital, B., & Siong, S. C. (2006). Parametric effects of numerical distance on the intraparietal sulcus during passive viewing of rapid numerosity changes. *Brain Research*, 1067(1), 181–188. <https://doi.org/10.1016/j.brainres.2005.10.083>
- Ashburner, J. (2007). A fast diffeomorphic image registration algorithm. *NeuroImage*, 38(1), 95–113. <https://doi.org/10.1016/j.neuroimage.2007.07.007>
- Badre, D., & D'Esposito, M. (2007). Functional magnetic resonance imaging evidence for a hierarchical organization of the prefrontal cortex. *Journal of Cognitive Neuroscience*, 19(12), 2082–2099. <https://doi.org/10.1162/jocn.2007.19.12.2082>
- Badre, D., & Nee, D. E. (2018). Frontal cortex and the hierarchical control of behavior. *Trends in Cognitive Sciences*, 22(2), 170–188. <https://doi.org/10.1016/j.tics.2017.11.005>
- Badre, D., & Wagner, A. D. (2004). Selection, integration, and conflict monitoring. *Neuron*, 41(3), 473–487. [https://doi.org/10.1016/s0896-6273\(03\)00851-1](https://doi.org/10.1016/s0896-6273(03)00851-1)
- Baggio, H. C., Segura, B., Junque, C., de Reus, M. A., Sala-Llonch, R., & Van den Heuvel, M. P. (2015). Rich club organization and cognitive performance in healthy older participants. *Journal of Cognitive Neuroscience*, 27(9), 1801–1810. https://doi.org/10.1162/jocn_a_00821
- Ball, G., Aljabar, P., Zebari, S., Tusor, N., Arichi, T., Merchant, N., Robinson, E. C., Ogunidipe, E., Rueckert, D., Edwards, A. D., & Counsell, S. J. (2014). Rich-club organization of the newborn human brain. *Proceedings of the National Academy of Sciences of the United States of America*, 111(20), 7456–7461. <https://doi.org/10.1073/pnas.1324118111>
- Bassett, D. S., Brown, J. A., Deshpande, V., Carlson, J. M., & Grafton, S. T. (2011). Conserved and variable architecture of human white matter connectivity. *NeuroImage*, 54(2), 1262–1279. <https://doi.org/10.1016/j.neuroimage.2010.09.006>
- Bassett, D. S., Bullmore, E., Verchinski, B. A., Mattay, V. S., Weinberger, D. R., & Meyer-Lindenberg, A. (2008). Hierarchical organization of human cortical networks in health and schizophrenia. *Journal of Neuroscience*, 28(37), 9239–9248. <https://doi.org/10.1523/JNEUROSCI.1929-08.2008>
- Bathelt, J., Gathercole, S. E., Butterfield, S., & Astle, D. E. (2018). Children's academic attainment is linked to the global organization of the white matter connectome. *Developmental Science*, 21(5), 1–14. <https://doi.org/10.1111/desc.12662>
- Benjamini, Y., & Hochberg, Y. (1995). Controlling the false discovery rate: A practical and powerful approach to multiple testing. *Journal of the Royal Statistical Society*, 57(1), 289–300.
- Bertolero, M. A., Yeo, B. T. T., & D'Esposito, M. (2017). The diverse club. *Nature Communications*, 8(1), 1–10. <https://doi.org/10.1038/s41467-017-01189-w>
- Bick, C., & Rabinovich, M. I. (2009). Dynamical origin of the effective storage capacity in the brain's working memory. *Physical Review Letters*, 103(21), 1–4. <https://doi.org/10.1103/PhysRevLett.103.218101>
- Bor, D., & Seth, A. K. (2012). Consciousness and the prefrontal parietal network: Insights from attention, working memory, and chunking. *Frontiers in Psychology*, 3(MAR), 1–14. <https://doi.org/10.3389/fpsyg.2012.00063>
- Botvinick, M. M. (2008). Hierarchical models of behavior and prefrontal function. *Trends in Cognitive Sciences*, 12(5), 201–208. <https://doi.org/10.1016/j.tics.2008.02.009>
- Braun, U., Plichta, M. M., Esslinger, C., Sauer, C., Haddad, L., Grimm, O., Mier, D., Mohnke, S., Heinz, A., Erk, S., Walter, H., Seifarth, N., Kirsch, P., & Meyer-Lindenberg, A. (2012). Test-retest reliability of resting-state connectivity network characteristics using fMRI and graph theoretical measures. *NeuroImage*, 59(2), 1404–1412. <https://doi.org/10.1016/j.neuroimage.2011.08.044>
- Brimijoin, W. O., & O'Neill, W. E. (2010). Patterned tone sequences reveal non-linear interactions in auditory spectrotemporal receptive fields in the inferior colliculus. *Hearing Research*, 267(1–2), 96–110. <https://doi.org/10.1016/j.heares.2010.04.005>
- Brown, J. A., Terashima, K. H., Burggren, A. C., Ercoli, L. M., Miller, K. J., Small, G. W., & Bookheimer, S. Y. (2011). Brain network local interconnectivity loss in aging APOE-4 allele carriers. *Proceedings of the National Academy of Sciences of the United States of America*, 108(51), 20760–20765. <https://doi.org/10.1073/pnas.1109038108>
- Brunia, C. H. M. (1999). Neural aspects of anticipatory behavior. *Acta Psychologica*, 101(2–3), 213–242. [https://doi.org/10.1016/s0001-6918\(99\)00006-2](https://doi.org/10.1016/s0001-6918(99)00006-2)
- Brybaert, M. (1995). Arabic number reading: On the nature of the numerical scale and the origin of phonological recoding. *Journal of Experimental Psychology: General*, 124(4), 434–452. <https://doi.org/10.1037/0096-3445.124.4.434>
- Bryce, N. V., Flournoy, J. C., Guassi Moreira, J. F., Rosen, M. L., Sambook, K. A., Mair, P., & McLaughlin, K. A. (2021). Brain parcellation selection: An overlooked decision point with meaningful effects on individual differences in resting-state functional connectivity. *NeuroImage*, 243(March), 118487. <https://doi.org/10.1016/j.neuroimage.2021.118487>
- Bürkner, P. C. (2017). Brms: An R package for Bayesian multilevel models using Stan. *Journal of Statistical Software*, 80(1), 1–28. <https://doi.org/10.18637/jss.v080.i01>
- Bürkner, P. C. (2018). Is the evidence ratio for a one sided hypothesis equivalent to a one sided Bayes factor? Retrieved from <https://github.com/paul-buerkner/brms/issues/311>
- Bussey, T. J., & Saksida, L. M. (2005). Object memory and perception in the medial temporal lobe: An alternative approach. *Current Opinion in Neurobiology*, 15(6), 730–737. <https://doi.org/10.1016/j.conb.2005.10.014>
- Calamante, F. (2019). The seven deadly sins of measuring brain structural connectivity using diffusion MRI streamlines fibre-tracking. *Diagnostics*, 9(3), 1–17. <https://doi.org/10.3390/diagnostics9030115>

- Cammoun, L., Gigandet, X., Meskaldji, D., Thiran, J. P., Sporns, O., Do, K. Q., Maeder, P., Meuli, R., & Hagmann, P. (2012). Mapping the human connectome at multiple scales with diffusion spectrum MRI. *Journal of Neuroscience Methods*, 203(2), 386–397. <https://doi.org/10.1016/j.jneumeth.2011.09.031>
- Cao, H., Plichta, M. M., Schäfer, A., Haddad, L., Grimm, O., Schneider, M., Esslinger, C., Kirsch, P., Meyer-Lindenberg, A., & Tost, H. (2014). Test-retest reliability of fMRI-based graph theoretical properties during working memory, emotion processing, and resting state. *NeuroImage*, 84, 888–900. <https://doi.org/10.1016/j.neuroimage.2013.09.013>
- Cao, Q., Shu, N., An, L., Wang, P., Sun, L., Xia, M. R., Wang, J. H., Gong, G. L., Zang, Y. F., Wang, Y. F., & He, Y. (2013). Probabilistic diffusion tractography and graph theory analysis reveal abnormal white matter structural connectivity networks in drug-naïve boys with attention deficit/hyperactivity disorder. *Journal of Neuroscience*, 33(26), 10676–10687. <https://doi.org/10.1523/JNEUROSCI.4793-12.2013>
- Cao, R., Wang, X., Gao, Y., Li, T., Zhang, H., Hussain, W., Xie, Y., Wang, J., Wang, B., & Xiang, J. (2020). Abnormal anatomical rich-club organization and structural–functional coupling in mild cognitive impairment and Alzheimer's disease. *Frontiers in Neurology*, 11(February), 1–17. <https://doi.org/10.3389/fneur.2020.00053>
- Chanes, L., & Feldman Barrett, L. (2016). Redefining the role of limbic areas in cortical processing. *Trends in Cognitive Sciences*, 20(2), 96–106. <https://doi.org/10.1016/j.tics.2015.11.005>
- Chang, L.-C., Jones, D. K., & Pierpaoli, C. (2005). RESTORE: Robust estimation of tensors by outlier rejection. *Magnetic Resonance in Medicine*, 53(5), 1088–1095. <https://doi.org/10.1002/mrm.20426>
- Chang, L.-C., Walker, L., & Pierpaoli, C. (2012). Informed RESTORE: A method for robust estimation of diffusion tensor from low redundancy datasets in the presence of physiological noise artifacts. *Magnetic Resonance in Medicine*, 68(5), 1654–1663. <https://doi.org/10.1002/mrm.24173>
- Chen, J., Leong, Y. C., Honey, C. J., Yong, C. H., Norman, K. A., & Hasson, U. (2017). Shared memories reveal shared structure in neural activity across individuals. *Nature Neuroscience*, 20(1), 115–125. <https://doi.org/10.1038/nn.4450>
- Chen, Z., Liu, M., Gross, D. W., & Beaulieu, C. (2013). Graph theoretical analysis of developmental patterns of the white matter network. *Frontiers in Human Neuroscience*, 7(NOV), 1–13. <https://doi.org/10.3389/fnhum.2013.00716>
- Chung, M. K., Lee, H., Solo, V., Davidson, R. J., & Pollak, S. D. (2017). Topological distances between brain networks. *Lecture Notes in Computer Science*, 10511, 161–170. https://doi.org/10.1007/978-3-319-67159-8_19
- Colizza, V., Flammini, A., Serrano, M. A., & Vespignani, A. (2006). Detecting rich-club ordering in complex networks. *Nature Physics*, 2(2), 110–115. <https://doi.org/10.1038/nphys209>
- Collin, G., Kahn, R. S., De Reus, M. A., Cahn, W., & van den Heuvel, M. P. (2014). Impaired rich club connectivity in unaffected siblings of schizophrenia patients. *Schizophrenia Bulletin*, 40(2), 438–448. <https://doi.org/10.1093/schbul/sbt162>
- Collin, G., Scholtens, L. H., Kahn, R. S., Hillegers, M. H. J., & van den Heuvel, M. P. (2017). Affected anatomical rich club and structural–functional coupling in young offspring of schizophrenia and bipolar disorder patients. *Biological Psychiatry*, 82(10), 746–755. <https://doi.org/10.1016/j.biopsych.2017.06.013>
- Collin, G., Sporns, O., Mandl, R. C. W., & Van Den Heuvel, M. P. (2014). Structural and functional aspects relating to cost and benefit of rich club organization in the human cerebral cortex. *Cerebral Cortex*, 24(9), 2258–2267. <https://doi.org/10.1093/cercor/bht064>
- Corbin, N., Todd, N., Friston, K. J., & Callaghan, M. F. (2018). Accurate modeling of temporal correlations in rapidly sampled fMRI time series. *Human Brain Mapping*, 39(10), 3884–3897. <https://doi.org/10.1002/hbm.24218>
- Craddock, R. C., James, G. A., Holtzheimer, P. E., Hu, X. P., & Mayberg, H. S. (2012). A whole brain fMRI atlas generated via spatially constrained spectral clustering. *Human Brain Mapping*, 33(8), 1914–1928. <https://doi.org/10.1002/hbm.21333>
- Cramer, D., & Howitt, D. (2011). *The SAGE dictionary of statistics*. SAGE Publications. <https://doi.org/10.4135/9780857020123>
- Crittenden, B. M., & Duncan, J. (2014). Task difficulty manipulation reveals multiple demand activity but no frontal lobe hierarchy. *Cerebral Cortex*, 24(2), 532–540. <https://doi.org/10.1093/cercor/bhs333>
- Crossley, N. A., Mechelli, A., Scott, J., Carletti, F., Fox, P. T., McGuire, P., & Bullmore, E. T. (2014). The hubs of the human connectome are generally implicated in the anatomy of brain disorders. *Brain*, 137(8), 2382–2395. <https://doi.org/10.1093/brain/awu132>
- Crossley, N. A., Mechelli, A., Vértes, P. E., Winton-Brown, T. T., Patel, A. X., Ginestet, C. E., McGuire, P., & Bullmore, E. T. (2013). Cognitive relevance of the community structure of the human brain functional coactivation network. *Proceedings of the National Academy of Sciences of the United States of America*, 110(28), 11583–11588. <https://doi.org/10.1073/pnas.1220826110>
- Cui, H. (2014). From intention to action: Hierarchical sensorimotor transformation in the posterior parietal cortex. *ENeuro*, 1(1), 1–6. <https://doi.org/10.1523/ENEURO.0017-14.2014>
- Cullen, A. C., & Frey, H. C. (1999). *Probabilistic techniques in exposure assessment: A handbook for dealing with variability and uncertainty in models and inputs*. Springer Science+Business Media.
- de Bruijn, G. N. (1946). A combinatorial problem. *Proceedings of the Koninklijke Nederlandse Akademie van Wetenschappen*, 49, 758–764. Retrieved from <http://ci.nii.ac.jp/naid/10019660672/en/>
- de Lange, S. C., Helwegen, K., & van den Heuvel, M. P. (2023). Structural and functional connectivity reconstruction with CATO—A connectivity analysis TOOLbox. *NeuroImage*, 273(April), 120108. <https://doi.org/10.1016/j.neuroimage.2023.120108>
- de Reus, M. A., & van den Heuvel, M. P. (2013a). Estimating false positives and negatives in brain networks. *NeuroImage*, 70, 402–409. <https://doi.org/10.1016/j.neuroimage.2012.12.066>
- de Reus, M. A., & van den Heuvel, M. P. (2013b). The parcellation-based connectome: Limitations and extensions. *NeuroImage*, 80, 397–404. <https://doi.org/10.1016/j.neuroimage.2013.03.053>
- Dehaene, S., Piazza, M., Pinel, P., & Cohen, L. (2003). Three parietal circuits for number processing. *Cognitive Neuropsychology*, 20(3–6), 487–506. <https://doi.org/10.1080/02643290244000239>
- Desikan, R. S., Ségonne, F., Fischl, B., Quinn, B. T., Dickerson, B. C., Blacker, D., Buckner, R. L., Dale, A. M., Maguire, R. P., Hyman, B. T., Albert, M. S., & Killiany, R. J. (2006). An automated labeling system for subdividing the human cerebral cortex on MRI scans into gyral based regions of interest. *NeuroImage*, 31(3), 968–980. <https://doi.org/10.1016/j.neuroimage.2006.01.021>
- Diedenhofen, B., & Musch, J. (2015). Cocor: A comprehensive solution for the statistical comparison of correlations. *PLoS One*, 10(4), 1–12. <https://doi.org/10.1371/journal.pone.0121945>
- Dixon, M. L., Girn, M., & Christoff, K. (2017). Hierarchical organization of frontoparietal control networks underlying goal-directed behavior. In *The prefrontal cortex as an executive, emotional, and social brain* (pp. 133–148). Springer Japan. https://doi.org/10.1007/978-4-431-56508-6_7
- Dormal, V., Dormal, G., Joassin, F., & Pesenti, M. (2012). A common right fronto-parietal network for numerosity and duration processing: An fMRI study. *Human Brain Mapping*, 33(6), 1490–1501. <https://doi.org/10.1002/hbm.21300>
- Dunn, O. J., & Clark, V. (1969). Correlation coefficients measured on the same individuals. *Journal of the American Statistical Association*, 64(325), 366–377. <https://doi.org/10.1080/01621459.1969.10500981>
- Fallon, J., Ward, P. G. D., Parkes, L., Oldham, S., Arnatkevičiūtė, A., Fornito, A., & Fulcher, B. D. (2020). Timescales of spontaneous fMRI

- fluctuations relate to structural connectivity in the brain. *Network Neuroscience*, 4(3), 788–806. https://doi.org/10.1162/netn_a_00151
- Farbood, M. M., Heeger, D. J., Marcus, G., Hasson, U., & Lerner, Y. (2015). The neural processing of hierarchical structure in music and speech at different timescales. *Frontiers in Neuroscience*, 9(APR), 1–13. <https://doi.org/10.3389/fnins.2015.00157>
- Fischl, B. (2012). FreeSurfer. *NeuroImage*, 62(2), 774–781. <https://doi.org/10.1016/j.neuroimage.2012.01.021>
- Fitch, W. T., & Martins, M. D. (2014). Hierarchical processing in music, language, and action: Lashley revisited. *Annals of the New York Academy of Sciences*, 1316(1), 87–104. <https://doi.org/10.1111/nyas.12406>
- Fornito, A., Zalesky, A., & Bullmore, E. (2016). *Fundamentals of brain network analysis*. Elsevier. <https://doi.org/10.1016/C2012-0-06036-X>
- Fukushima, M., Betzel, R. F., He, Y., van den Heuvel, M. P., Zuo, X. N., & Sporns, O. (2018). Structure–function relationships during segregated and integrated network states of human brain functional connectivity. *Brain Structure and Function*, 223(3), 1091–1106. <https://doi.org/10.1007/s00429-017-1539-3>
- Fuster, J. M. (2001). The prefrontal cortex—An update: Time is of the essence. *Neuron*, 30(2), 319–333. [https://doi.org/10.1016/S0896-6273\(01\)00285-9](https://doi.org/10.1016/S0896-6273(01)00285-9)
- Fuster, J. M., & Bressler, S. L. (2015). Past makes future: Role of pFC in prediction. *Journal of Cognitive Neuroscience*, 27(4), 639–654. https://doi.org/10.1162/jocn_a_00746
- Gao, R., van den Brink, R. L., Pfeffer, T., & Voytek, B. (2020). Neuronal timescales are functionally dynamic and shaped by cortical microarchitecture. *eLife*, 9, 1–26. <https://doi.org/10.7554/eLife.61277>
- Genovesio, A., Wise, S. P., & Passingham, R. E. (2014). Prefrontal–parietal function: from foraging to foresight. *Trends in Cognitive Sciences*, 18(2), 72–81. <https://doi.org/10.1016/j.tics.2013.11.007>
- Glasser, M. F., Coalson, T. S., Robinson, E. C., Hacker, C. D., Harwell, J., Yacoub, E., Ugurbil, K., Andersson, J., Beckmann, C. F., Jenkinson, M., Smith, S. M., & Van Essen, D. C. (2016). A multi-modal parcellation of human cerebral cortex. *Nature*, 536(7615), 171–178. <https://doi.org/10.1038/nature18933>
- Goffin, C. (2019). How does the brain represent digits? Investigating the neural correlates of symbolic number representation using fMRI—Adaptation [The University of Western Ontario]. Retrieved from <https://ir.lib.uwo.ca/etd/6613>
- Golde, M., von Cramon, D. Y., & Schubotz, R. I. (2010). Differential role of anterior prefrontal and premotor cortex in the processing of relational information. *NeuroImage*, 49(3), 2890–2900. <https://doi.org/10.1016/j.neuroimage.2009.09.009>
- Golesorkhi, M., Gomez-Pilar, J., Tumati, S., Northoff, G., Fraser, M., & Northoff, G. (2021). Temporal hierarchy of intrinsic neural timescales converges with spatial core-periphery organization. *Communications Biology*, 4(1), 1–14. <https://doi.org/10.1038/s42003-021-01785-z>
- Golesorkhi, M., Gomez-Pilar, J., Zilio, F., Berberian, N., Wolff, A., Yagoub, M. C. E., & Northoff, G. (2021). The brain and its time: Intrinsic neural timescales are key for input processing. *Communications Biology*, 4(1), 1–16. <https://doi.org/10.1038/s42003-021-02483-6>
- Gollo, L. L., Zalesky, A., Matthew Hutchison, R., van den Heuvel, M. P., & Breakspear, M. (2015). Dwelling quietly in the rich club: Brain network determinants of slow cortical fluctuations. *Philosophical Transactions of the Royal Society B: Biological Sciences*, 370(1668), 20140165. <https://doi.org/10.1098/rstb.2014.0165>
- Gómez, C. M., Vaquero, E., & Vázquez-Marrufo, M. (2004). A neurocognitive model for short-term sensory and motor preparatory activity in humans. *Psicológica*, 25(2), 217–229. <https://www.redalyc.org/articulo.oa?id=16925206>
- Gómez-Gardeñes, J., Zamora-López, G., Moreno, Y., & Arenas, A. (2010). From modular to centralized organization of synchronization in functional areas of the cat cerebral cortex. *PLoS One*, 5(8), e12313. <https://doi.org/10.1371/journal.pone.0012313>
- Goulas, A., Uylings, H. B. M., & Stiers, P. (2014). Mapping the hierarchical layout of the structural network of the macaque prefrontal cortex. *Cerebral Cortex*, 24(5), 1178–1194. <https://doi.org/10.1093/cercor/bhs399>
- Grafton, S. T., & Hamilton, A. F. D. C. (2007). Evidence for a distributed hierarchy of action representation in the brain. *Human Movement Science*, 26(4), 590–616. <https://doi.org/10.1016/j.humov.2007.05.009>
- Graybiel, A. M. (2008). Habits, rituals, and the evaluative brain. *Annual Review of Neuroscience*, 31, 359–387. <https://doi.org/10.1146/annurev.neuro.29.051605.112851>
- Grayson, D. S., Ray, S., Carpenter, S., Iyer, S., Dias, T. G. C., Stevens, C., Nigg, J. T., & Fair, D. A. (2014). Structural and functional rich club organization of the brain in children and adults. *PLoS One*, 9(2), 1–13. <https://doi.org/10.1371/journal.pone.0088297>
- Griffa, A., Baumann, P. S., Thiran, J. P., & Hagmann, P. (2013). Structural connectomics in brain diseases. *NeuroImage*, 80, 515–526. <https://doi.org/10.1016/j.neuroimage.2013.04.056>
- Griffa, A., & van den Heuvel, M. P. (2018). Rich-club neurocircuitry: Function, evolution, and vulnerability. *Dialogues in Clinical Neuroscience*, 20(2), 121–132. <https://doi.org/10.31887/dcn.2018.20.2/agriffa>
- Guimerà, R., & Nunes Amaral, L. A. (2005). Functional cartography of complex metabolic networks. *Nature*, 433(7028), 895–900. <https://doi.org/10.1038/nature03288>
- Hagmann, P., Cammoun, L., Gigandet, X., Meuli, R., Honey, C. J., Van Wvedeen, J., & Sporns, O. (2008). Mapping the structural core of human cerebral cortex. *PLoS Biology*, 6(7), 1479–1493. <https://doi.org/10.1371/journal.pbio.0060159>
- Hagmann, P., Sporns, O., Madan, N., Cammoun, L., Pienaar, R., Wedeen, V. J., Meuli, R., Thiran, J. P., & Grant, P. E. (2010). White matter maturation reshapes structural connectivity in the late developing human brain. *Proceedings of the National Academy of Sciences of the United States of America*, 107(44), 19067–19072. <https://doi.org/10.1073/pnas.1009073107>
- Hamilton, A. F. D. C., & Grafton, S. T. (1993). The motor hierarchy: from kinematics to goals and intentions. In *Sensorimotor foundations of higher cognition* (pp. 381–407). Oxford University Press. <https://doi.org/10.1093/acprof:oso/9780199231447.003.0018>
- Hansen, J. Y., Shafiei, G., Voigt, K., Liang, E. X., Cox, S. M. L., Leyton, M., Jamadar, S. D., & Misisic, B. (2022). Multimodal, multiscale connectivity blueprints of the cerebral cortex. *BioRxiv*, 2022.12.02.518906. Retrieved from <https://www.biorxiv.org/content/10.1101/2022.12.02.518906v1.abstract>
- Harriger, L., van den Heuvel, M. P., & Sporns, O. (2012). Rich club organization of macaque cerebral cortex and its role in network communication. *PLoS One*, 7(9), e46497. <https://doi.org/10.1371/journal.pone.0046497>
- Harrison, L. M., Duggins, A., & Friston, K. J. (2006). Encoding uncertainty in the hippocampus. *Neural Networks*, 19(5), 535–546. <https://doi.org/10.1016/j.neunet.2005.11.002>
- Hasson, U., Chen, J., & Honey, C. J. (2015). Hierarchical process memory: Memory as an integral component of information processing. *Trends in Cognitive Sciences*, 19(6), 304–313. <https://doi.org/10.1016/j.tics.2015.04.006>
- Hasson, U., Malach, R., & Heeger, D. J. (2010). Reliability of cortical activity during natural stimulation. *Trends in Cognitive Sciences*, 14(1), 40–48. <https://doi.org/10.1016/j.tics.2009.10.011>
- Hasson, U., Yang, E., Vallines, I., Heeger, D. J., & Rubin, N. (2008). A hierarchy of temporal receptive windows in human cortex. *Journal of Neuroscience*, 28(10), 2539–2550. <https://doi.org/10.1523/JNEUROSCI.5487-07.2008>
- Hermundstad, A. M., Bassett, D. S., Brown, K. S., Aminoff, E. M., Clewett, D., Freeman, S., Frithsen, A., Johnson, A., Tipper, C. M., Miller, M. B., Grafton, S. T., & Carlson, J. M. (2013). Structural foundations of resting-state and task-based functional connectivity in the human brain. *Proceedings of the National Academy of Sciences of*

- the United States of America, 110(15), 6169–6174. <https://doi.org/10.1073/pnas.1219562110>
- Hilgetag, C. C., Medalla, M., Beul, S. F., & Barbas, H. (2016). The primate connectome in context: Principles of connections of the cortical visual system. *NeuroImage*, 134, 685–702. <https://doi.org/10.1016/j.neuroimage.2016.04.017>
- Hittner, J. B., May, K., & Silver, N. C. (2003). A Monte Carlo evaluation of tests for comparing dependent correlations. *Journal of General Psychology*, 130(2), 149–168. <https://doi.org/10.1080/00221300309601282>
- Huang, H., Shu, N., Mishra, V., Jeon, T., Chalak, L., Wang, Z. J., Rollins, N., Gong, G., Cheng, H., Peng, Y., Dong, Q., & He, Y. (2015). Development of human brain structural networks through infancy and childhood. *Cerebral Cortex*, 25(5), 1389–1404. <https://doi.org/10.1093/cercor/bht335>
- Ingvar, D. H. (1985). "Memory of the future": An essay on the temporal organization of conscious awareness. *Human Neurobiology*, 4(3), 127–136.
- Ito, T., Hearne, L. J., & Cole, M. W. (2020). A cortical hierarchy of localized and distributed processes revealed via dissociation of task activations, connectivity changes, and intrinsic timescales. *NeuroImage*, 221(July), 117141. <https://doi.org/10.1016/j.neuroimage.2020.117141>
- Jao, C.-W., Yeh, J.-H., Wu, Y.-T., Lien, L.-M., Tsai, Y.-F., Chu, K.-E., Hsiao, C.-Y., Wang, P.-S., & Lau, C. I. (2020). Alteration of the intra- and inter-lobe connectivity of the brain structural network in normal aging. *Entropy*, 22(8), 826. <https://doi.org/10.3390/e22080826>
- Jarret, J., Boré, A., Bedetti, C., Descoteaux, M., & Brambati, S. M. (2022). A methodological scoping review of the integration of fMRI to guide dmRI tractography. What has been done and what can be improved: A 20-year perspective. *Journal of Neuroscience Methods*, 367, 109435. <https://doi.org/10.1016/j.jneumeth.2021.109435>
- Jenkinson, M., Beckmann, C. F., Behrens, T. E. J., Woolrich, M. W., & Smith, S. M. (2012). Fsl. *NeuroImage*, 62, 782–790. <https://doi.org/10.1016/j.neuroimage.2011.09.015>
- Jeon, H. A. (2014). Hierarchical processing in the prefrontal cortex in a variety of cognitive domains. *Frontiers in Systems Neuroscience*, 8(NOV), 1–8. <https://doi.org/10.3389/fnsys.2014.00223>
- Jones, D. K., Knösche, T. R., & Turner, R. (2013). White matter integrity, fiber count, and other fallacies: The do's and don'ts of diffusion MRI. *NeuroImage*, 73, 239–254. <https://doi.org/10.1016/j.neuroimage.2012.06.081>
- Kai, J., Khan, A. R., Haast, R. A., & Lau, J. C. (2022). Mapping the subcortical connectome using in vivo diffusion MRI: Feasibility and reliability. *NeuroImage*, 262(March), 119553. <https://doi.org/10.1016/j.neuroimage.2022.119553>
- Keown, C. L., Datko, M. C., Chen, C. P., Maximo, J. O., Jahedi, A., & Müller, R.-A. (2017). Network organization is globally atypical in autism: A graph theory study of intrinsic functional connectivity. *Biological Psychiatry: Cognitive Neuroscience and Neuroimaging*, 2(1), 66–75. <https://doi.org/10.1016/j.bpsc.2016.07.008>
- Kiebel, S. J., Daunizeau, J., & Friston, K. J. (2008). A hierarchy of time-scales and the brain. *PLoS Computational Biology*, 4(11), e1000209. <https://doi.org/10.1371/journal.pcbi.1000209>
- Kim, D. J., Davis, E. P., Sandman, C. A., Sporns, O., O'Donnell, B. F., Buss, C., & Hetrick, W. P. (2016). Children's intellectual ability is associated with structural network integrity. *NeuroImage*, 124, 550–556. <https://doi.org/10.1016/j.neuroimage.2015.09.012>
- Kocher, M., Gleichgerrcht, E., Nesland, T., Rorden, C., Fridriksson, J., Spampinato, M. v., & Bonilha, L. (2015). Individual variability in the anatomical distribution of nodes participating in rich club structural networks. *Frontiers in Neural Circuits*, 9(APR), 1–7. <https://doi.org/10.3389/fncir.2015.00016>
- Koechlin, E., Basso, G., Pietrini, P., Panzer, S., & Grafman, J. (1999). The role of the anterior prefrontal cortex in human cognition. *Nature*, 399(6732), 148–151. <https://doi.org/10.1038/20178>
- Koechlin, E., & Summerfield, C. (2007). An information theoretical approach to prefrontal executive function. *Trends in Cognitive Sciences*, 11(6), 229–235. <https://doi.org/10.1016/j.tics.2007.04.005>
- Kravitz, D. J., Saleem, K. S., Baker, C. I., Ungerleider, L. G., & Mishkin, M. (2013). The ventral visual pathway: An expanded neural framework for the processing of object quality. *Trends in Cognitive Sciences*, 17(1), 26–49. <https://doi.org/10.1016/j.tics.2012.10.011>
- Kriegeskorte, N., Simmons, W. K., Bellgowan, P. S., & Baker, C. I. (2009). Circular analysis in systems neuroscience: The dangers of double dipping. *Nature Neuroscience*, 12(5), 535–540. <https://doi.org/10.1038/nn.2303>
- Kühn, A. B., & Schubotz, R. I. (2012). Temporally remote destabilization of prediction after rare breaches of expectancy. *Human Brain Mapping*, 33(8), 1812–1820. <https://doi.org/10.1002/hbm.21325>
- Landis, J. R., & Koch, G. G. (1977). The measurement of observer agreement for categorical data. *Biometrics*, 33(1), 159. <https://doi.org/10.2307/2529310>
- Lee, W. J., Han, C. E., Aganj, I., Seo, S. W., & Seong, J. K. (2018). Distinct patterns of rich club organization in Alzheimer's disease and subcortical vascular dementia: A white matter network study. *Journal of Alzheimer's Disease*, 63(3), 977–987. <https://doi.org/10.3233/JAD-180027>
- Lerner, Y., Honey, C. J., Silbert, L. J., & Hasson, U. (2011). Topographic mapping of a hierarchy of temporal receptive windows using a narrated story. *Journal of Neuroscience*, 31(8), 2906–2915. <https://doi.org/10.1523/JNEUROSCI.3684-10.2011>
- Liu, Y., Yang, K., Hu, X., Xiao, C., Rao, J., Li, Z., Liu, D., Zou, Y., Chen, J., & Liu, H. (2020). Altered rich-club organization and regional topology are associated with cognitive decline in patients with frontal and temporal gliomas. *Frontiers in Human Neuroscience*, 14(February), 1–13. <https://doi.org/10.3389/fnhum.2020.00023>
- Lurie, D. J., Pappas, I., Esposito, M. D., Lurie, D. J., & D'Esposito, M. (2023). Cortical timescales and the modular organization of structural and functional brain networks. *BioRxiv*. <https://doi.org/10.1101/2023.07.12.548751>
- Ma, J., Kang, H. J., Kim, J. Y., Jeong, H. S., Im, J. J., Namgung, E., Kim, M. J., Lee, S., Kim, T. D., Oh, J. K., Chung, Y. A., Lyoo, I. K., Lim, S. M., & Yoon, S. (2017). Network attributes underlying intellectual giftedness in the developing brain. *Scientific Reports*, 7(1), 1–9. <https://doi.org/10.1038/s41598-017-11593-3>
- Mahjoory, K., Schoffelen, J. M., Keitel, A., & Gross, J. (2020). The frequency gradient of human resting-state brain oscillations follows cortical hierarchies. *eLife*, 9, 1–18. <https://doi.org/10.7554/ELIFE.53715>
- Maldjian, J. A., Laurienti, P. J., Kraft, R. A., & Burdette, J. H. (2003). An automated method for neuroanatomic and cytoarchitectonic atlas-based interrogation of fMRI data sets. *NeuroImage*, 19(3), 1233–1239. [https://doi.org/10.1016/S1053-8119\(03\)00169-1](https://doi.org/10.1016/S1053-8119(03)00169-1)
- Miller, E. K., & Cohen, J. D. (2001). An integrative theory of prefrontal cortex function. *Annual Review of Neuroscience*, 24(1), 167–202. <https://doi.org/10.1146/annurev.neuro.24.1.167>
- Miller, G. A. (1956). The magical number seven, plus or minus two: Some limits on our capacity for processing information. *Psychological Review*, 63(2), 81–97. <https://doi.org/10.1037/h0043158>
- Mohor, G. S., Thieken, A. H., & Korup, O. (2021). Residential flood loss estimated from Bayesian multilevel models. *Natural Hazards and Earth System Sciences*, 21(5), 1599–1614. <https://doi.org/10.5194/nhess-21-1599-2021>
- Molko, N., Cachia, A., Rivière, D., Mangin, J. F., Bruandet, M., Le Bihan, D., Cohen, L., & Dehaene, S. (2003). Functional and structural alterations of the intraparietal sulcus in a developmental dyscalculia of genetic origin. *Neuron*, 40(4), 847–858. [https://doi.org/10.1016/S0896-6273\(03\)00670-6](https://doi.org/10.1016/S0896-6273(03)00670-6)
- Mori, S., Crain, B. J., Chacko, V. P., & van Zijl, P. C. M. (1999). Three-dimensional tracking of axonal projections in the brain by magnetic resonance imaging. *Annals of Neurology*, 45(2), 265–269. [https://doi.org/10.1002/1531-8249\(199902\)45:2<247::AID-ANA16>3.0.CO;2-U](https://doi.org/10.1002/1531-8249(199902)45:2<247::AID-ANA16>3.0.CO;2-U)
- Nattkemper, D., & Prinz, W. (1997). Stimulus and response anticipation in a serial reaction task. *Psychological Research*, 60(1–2), 98–112. <https://doi.org/10.1007/BF00419683>

- Naya, Y., Yoshida, M., & Miyashita, Y. (2003). Forward processing of long-term associative memory in monkey inferotemporal cortex. *Journal of Neuroscience*, 23(7), 2861–2871. <https://doi.org/10.1523/jneurosci.23-07-02861.2003>
- Nee, D. E., & D'Esposito, M. (2016). The hierarchical organization of the lateral prefrontal cortex. *eLife*, 5(MARCH2016), 1–26. <https://doi.org/10.7554/eLife.12112>
- Nieder, A. (2016). Representing Something Out of Nothing: The Dawning of Zero. *Trends in Cognitive Sciences*, 20(11), 830–842. <https://doi.org/10.1016/j.tics.2016.08.008>
- Noonan, K. A., Jefferies, E., Visser, M., & Lambon Ralph, M. A. (2013). Going beyond inferior prefrontal involvement in semantic control: Evidence for the additional contribution of dorsal angular gyrus and posterior middle temporal cortex. *Journal of Cognitive Neuroscience*, 25(11), 1824–1850. https://doi.org/10.1162/jocn_a_00442
- O'Donoghue, S., Kilmartin, L., O'Hara, D., Emsell, L., Langan, C., McInerney, S., Forde, N. J., Leemans, A., Jeurissen, B., Barker, G. J., McCarthy, P., Cannon, D. M., & McDonald, C. (2017). Anatomical integration and rich-club connectivity in euthymic bipolar disorder. *Psychological Medicine*, 47(9), 1609–1623. <https://doi.org/10.1017/S0033291717000058>
- Oldfield, R. C. (1971). The assessment and analysis of handedness: The Edinburgh inventory. *Neuropsychologia*, 9(9), 97–113. https://doi.org/10.1007/978-3-319-55065-7_301010
- Patriat, R., Molloy, E. K., Meier, T. B., Kirk, G. R., Nair, V. A., Meyerand, M. E., Prabhakaran, V., & Birn, R. M. (2013). The effect of resting condition on resting-state fMRI reliability and consistency: A comparison between resting with eyes open, closed, and fixated. *NeuroImage*, 78, 463–473. <https://doi.org/10.1016/j.neuroimage.2013.04.013>
- Pedersen, M., Omidvarnia, A., Shine, J. M., Jackson, G. D., & Zalesky, A. (2020). Reducing the influence of intramodular connectivity in participation coefficient. *Network Neuroscience*, 4(2), 416–431. https://doi.org/10.1162/netn_a_00127
- Piazza, M., Izard, V., Pinel, P., Le Bihan, D., & Dehaene, S. (2004). Tuning curves for approximate numerosity in the human intraparietal sulcus. *Neuron*, 44(3), 547–555. <https://doi.org/10.1016/j.neuron.2004.10.014>
- Piazza, M., Pinel, P., Le Bihan, D., & Dehaene, S. (2007). A magnitude code common to numerosities and number symbols in human intraparietal cortex. *Neuron*, 53(2), 293–305. <https://doi.org/10.1016/j.neuron.2006.11.022>
- Pinhas, M., & Tzelgov, J. (2012). Expanding on the mental number line: zero is perceived as the “smallest”. *Journal of Experimental Psychology: Learning, Memory, and Cognition*, 38(5), 1187–1205. <https://doi.org/10.1037/a0027390>
- Ponsoda, V., Martínez, K., Pineda-Pardo, J. A., Abad, F. J., Olea, J., Román, F. J., Barbey, A. K., & Colom, R. (2017). Structural brain connectivity and cognitive ability differences: A multivariate distance matrix regression analysis. *Human Brain Mapping*, 38(2), 803–816. <https://doi.org/10.1002/hbm.23419>
- Prčková, V., Rodrigues, P., Puigdellivol Sanchez, A., Ramos, M., Andorra, M., Martínez-Heras, E., Falcon, C., Prats-Galino, A., & Villoslada, P. (2016). Reproducibility of the structural connectome reconstruction across diffusion methods. *Journal of Neuroimaging*, 26(1), 46–57. <https://doi.org/10.1111/jon.12298>
- Qi, S., Meesters, S., Nicolay, K., ter Haar Romeny, B. M., & Ossenblok, P. (2015). The influence of construction methodology on structural brain network measures: A review. *Journal of Neuroscience Methods*, 253(500), 170–182. <https://doi.org/10.1016/j.jneumeth.2015.06.016>
- R Core Team. (2022). *R: A language and environment for statistical computing*. R Core Team Retrieved from <https://www.r-project.org/>
- Ramrani, N., & Owen, A. M. (2004). Anterior prefrontal cortex: Insights into function from anatomy and neuroimaging. *Nature Reviews Neuroscience*, 5(3), 184–194. <https://doi.org/10.1038/nrn1343>
- Raut, R. V., Snyder, A. Z., & Raichle, M. E. (2020). Hierarchical dynamics as a macroscopic organizing principle of the human brain. *Proceedings of the National Academy of Sciences of the United States of America*, 117(34), 20890–20897. <https://doi.org/10.1073/pnas.2003383117>
- Ray, S., Miller, M., Karalunas, S., Robertson, C., Grayson, D. S., Cary, R. P., Hawkey, E., Painter, J. G., Kriz, D., Fombonne, E., Nigg, J. T., & Fair, D. A. (2014). Structural and functional connectivity of the human brain in autism spectrum disorders and attention-deficit/hyperactivity disorder: A rich club-organization study. *Human Brain Mapping*, 35(12), 6032–6048. <https://doi.org/10.1002/hbm.22603>
- Reavis, E. A., Lee, J., Altshuler, L. L., Cohen, M. S., Engel, S. A., Glahn, D. C., Jimenez, A. M., Narr, K. L., Nuechterlein, K. H., Riedel, P., Wynn, J. K., & Green, M. F. (2020). Structural and functional connectivity of visual cortex in schizophrenia and bipolar disorder: A graph-theoretic analysis. *Schizophrenia Bulletin Open*, 1(1), 1–11. <https://doi.org/10.1093/schizbullopen/sgaa056>
- Repple, J., Mauritz, M., Meinert, S., de Lange, S. C., Grotegerd, D., Opel, N., Redlich, R., Hahn, T., Förster, K., Leehr, E. J., Winter, N., Goltermann, J., Enneking, V., Fingas, S. M., Lemke, H., Waltemate, L., Nenadic, I., Krug, A., Brosch, K., ... van den Heuvel, M. P. (2020). Severity of current depression and remission status are associated with structural connectome alterations in major depressive disorder. *Molecular Psychiatry*, 25(7), 1550–1558. <https://doi.org/10.1038/s41380-019-0603-1>
- Reynolds, J. R., O'Reilly, R. C., Cohen, J. D., & Braver, T. S. (2012). The function and organization of lateral prefrontal cortex: A test of competing hypotheses. *PLoS One*, 7(2), e30284. <https://doi.org/10.1371/journal.pone.0030284>
- Rhodes, S., Cowan, N., Parra, M. A., & Logie, R. H. (2019). Interaction effects on common measures of sensitivity: Choice of measure, type I error, and power. *Behavior Research Methods*, 51(5), 2209–2227. <https://doi.org/10.3758/s13428-018-1081-0>
- Riedel, L., van den Heuvel, M. P., & Markett, S. (2022). Trajectory of rich club properties in structural brain networks. *Human Brain Mapping*, 43(14), 4239–4253. <https://doi.org/10.1002/hbm.25950>
- RStudio Team. (2022). *RStudio: Integrated development environment for R*. RStudio Team Retrieved from <http://www.rstudio.com/>
- Rubinov, M., & Sporns, O. (2010). Complex network measures of brain connectivity: Uses and interpretations. *NeuroImage*, 52(3), 1059–1069. <https://doi.org/10.1016/j.neuroimage.2009.10.003>
- Sanides, F. (1964). Structure and function of the human frontal lobe. *Neuropsychologia*, 2(3), 209–219. [https://doi.org/10.1016/0028-3932\(64\)90005-3](https://doi.org/10.1016/0028-3932(64)90005-3)
- Schaefer, A., Kong, R., Gordon, E. M., Laumann, T. O., Zuo, X.-N., Holmes, A. J., Eickhoff, S. B., & Yeo, B. T. T. (2018). Local-global parcellation of the human cerebral cortex from intrinsic functional connectivity MRI. *Cerebral Cortex*, 28(9), 3095–3114. <https://doi.org/10.1093/cercor/bhx179>
- Seguin, C., Tian, Y., & Zalesky, A. (2020). Network communication models improve the behavioral and functional predictive utility of the human structural connectome. *Network Neuroscience*, 4(4), 980–1006. https://doi.org/10.1162/netn_a_00161
- Senden, M., Reuter, N., van den Heuvel, M. P., Goebel, R., & Deco, G. (2017). Cortical rich club regions can organize state-dependent functional network formation by engaging in oscillatory behavior. *NeuroImage*, 146, 561–574. <https://doi.org/10.1016/j.neuroimage.2016.10.044>
- Sethi, S. S., Zerbi, V., Wenderoth, N., Fornito, A., & Fulcher, B. D. (2017). Structural connectome topology relates to regional BOLD signal dynamics in the mouse brain. *Chaos*, 27(4), 047405. <https://doi.org/10.1063/1.4979281>
- Shafiei, G., Markello, R. D., De Wael, R. V., Bernhardt, B. C., Fulcher, B. D., & Misisic, B. (2020). Topographic gradients of intrinsic dynamics across neocortex. *eLife*, 9, 1–24. <https://doi.org/10.7554/eLife.62116>

- Shannon, C. E. (1948). A mathematical theory of communication. *Bell System Technical Journal*, 27(3), 379–423. <https://doi.org/10.1002/j.1538-7305.1948.tb01338.x>
- Shen, X., Tokoglu, F., Papademetris, X., & Constable, R. T. (2013). Group-wise whole-brain parcellation from resting-state fMRI data for network node identification. *NeuroImage*, 82, 403–415. <https://doi.org/10.1016/j.neuroimage.2013.05.081>
- Slotnick, S. D. (2017). Cluster success: fMRI inferences for spatial extent have acceptable false-positive rates. *Cognitive Neuroscience*, 8(3), 150–155. <https://doi.org/10.1080/17588928.2017.1319350>
- Slotnick, S. D., Moo, L. R., Segal, J. B., & Hart, J. (2003). Distinct prefrontal cortex activity associated with item memory and source memory for visual shapes. *Cognitive Brain Research*, 17(1), 75–82. [https://doi.org/10.1016/S0926-6410\(03\)00082-X](https://doi.org/10.1016/S0926-6410(03)00082-X)
- Smith, S. M., Jenkinson, M., Woolrich, M. W., Beckmann, C. F., Behrens, T. E. J., Johansen-Berg, H., Bannister, P. R., de Luca, M., Drobnjak, I., Flitney, D. E., Niazy, R. K., Saunders, J., Vickers, J., Zhang, Y., de Stefano, N., Brady, J. M., & Matthews, P. M. (2004). Advances in functional and structural MR image analysis and implementation as FSL. *NeuroImage*, 23(SUPPL. 1), 208–219. <https://doi.org/10.1016/j.neuroimage.2004.07.051>
- Sokolowski, H. M., Fias, W., Mousa, A., & Ansari, D. (2017). Common and distinct brain regions in both parietal and frontal cortex support symbolic and nonsymbolic number processing in humans: A functional neuroimaging meta-analysis. *NeuroImage*, 146, 376–394. <https://doi.org/10.1016/j.neuroimage.2016.10.028>
- Solé-Casals, J., Serra-Grabulosa, J. M., Romero-García, R., Vilaseca, G., Adan, A., Vilaró, N., Bargalló, N., & Bullmore, E. T. (2019). Structural brain network of gifted children has a more integrated and versatile topology. *Brain Structure and Function*, 224(7), 2373–2383. <https://doi.org/10.1007/s00429-019-01914-9>
- Sporns, O. (2011). The human connectome: A complex network. *Annals of the New York Academy of Sciences*, 1224(1), 109–125. <https://doi.org/10.1111/j.1749-6632.2010.05888.x>
- Sporns, O. (2013). Structure and function of complex brain networks. *Dialogues in Clinical Neuroscience*, 15(3), 247–262. <https://doi.org/10.31887/dcms.2013.15.3/osporns>
- Suárez, L. E., Markello, R. D., Betzel, R. F., & Misic, B. (2020). Linking structure and function in macroscale brain networks. *Trends in Cognitive Sciences*, 24(4), 302–315. <https://doi.org/10.1016/j.tics.2020.01.008>
- The MathWorks Inc. (2019). *MATLAB version: 9.6.0 (R2019a)*. The MathWorks Inc Retrieved from <https://www.mathworks.com>
- The MathWorks Inc. (2021). *MATLAB version: 9.10.0 (R2021a)*. The MathWorks Inc Retrieved from <https://www.mathworks.com>
- Tourbier, S., Aleman-Gomez, Y., Griffa, A., Bach Cuadra, M., & Hagmann, P. (2019). sebastientourbier/multiscalebrainparcellator: Multi-scale brain parcellator v1.1.1. <https://doi.org/10.5281/ZENODO.3627097>
- Uithol, S., van Rooij, I., Bekkering, H., & Haselager, P. (2012). Hierarchies in action and motor control. *Journal of Cognitive Neuroscience*, 24(5), 1077–1086. https://doi.org/10.1162/jocn_a_00204
- van den Heuvel, M. P., Kahn, R. S., Goñi, J., & Sporns, O. (2012). High-cost, high-capacity backbone for global brain communication. *Proceedings of the National Academy of Sciences of the United States of America*, 109(28), 11372–11377. <https://doi.org/10.1073/pnas.1203593109>
- van den Heuvel, M. P., Scholtens, L. H., van der Burgh, H. K., Agosta, F., Alloza, C., Arango, C., Auyeung, B., Baron-Cohen, S., Basaia, S., Benders, M. J. N. L., Beyer, F., Booij, L., Braun, K. P. J., Filho, G. B., Cahn, W., Cannon, D. M., Chaim-Avancini, T. M., Chan, S. S. M., Chen, E. Y. H., ... de Lange, S. C. (2019). 10kin1day: A bottom-up neuroimaging initiative. *Frontiers in Neurology*, 10(MAY), 1–7. <https://doi.org/10.3389/fneur.2019.00425>
- van den Heuvel, M. P., & Sporns, O. (2011). Rich-club organization of the human connectome. *Journal of Neuroscience*, 31(44), 15775–15786. <https://doi.org/10.1523/JNEUROSCI.3539-11.2011>
- van den Heuvel, M. P., & Sporns, O. (2013). Network hubs in the human brain. *Trends in Cognitive Sciences*, 17(12), 683–696. <https://doi.org/10.1016/j.tics.2013.09.012>
- van den Heuvel, M. P., Sporns, O., Collin, G., Scheewe, T., Mandl, R. C. W., Cahn, W., Goni, J., Pol, H. E. H., & Kahn, R. S. (2013). Abnormal rich club organization and functional brain dynamics in schizophrenia. *JAMA Psychiatry*, 70(8), 783–792. <https://doi.org/10.1001/jamapsychiatry.2013.1328>
- van Dijk, K. R. A., Hedden, T., Venkataraman, A., Evans, K. C., Lazar, S. W., & Buckner, R. L. (2010). Intrinsic functional connectivity as a tool for human connectomics: Theory, properties, and optimization. *Journal of Neurophysiology*, 103(1), 297–321. <https://doi.org/10.1152/jn.00783.2009>
- van Doorn, J., van den Bergh, D., Böhm, U., Dablander, F., Derks, K., Draws, T., Etz, A., Evans, N. J., Gronau, Q. F., Haaf, J. M., Hinne, M., Kucharský, Š., Ly, A., Marsman, M., Matzke, D., Gupta, A. R. K. N., Sarafoglou, A., Stefan, A., Voelkel, J. G., & Wagenmakers, E. J. (2021). The JASP guidelines for conducting and reporting a Bayesian analysis. *Psychonomic Bulletin and Review*, 28(3), 813–826. <https://doi.org/10.3758/s13423-020-01798-5>
- Van Essen, D. C., Smith, S. M., Barch, D. M., Behrens, T. E. J., Yacoub, E., & Ugurbil, K. (2013). The WU-Minn human connectome project: An overview. *NeuroImage*, 80, 62–79. <https://doi.org/10.1016/j.neuroimage.2013.05.041>
- Vogelbacher, C., Möbius, T. W. D., Sommer, J., Schuster, V., Dannlowski, U., Kircher, T., Dempfle, A., Jansen, A., & Bopp, M. H. A. (2018). The Marburg-Münster affective disorders cohort study (MACS): A quality assurance protocol for MR neuroimaging data. *NeuroImage*, 172(December 2017), 450–460. <https://doi.org/10.1016/j.neuroimage.2018.01.079>
- Wakita, M. (2014). Broca's area processes the hierarchical organization of observed action. *Frontiers in Human Neuroscience*, 7(JAN), 1–7. <https://doi.org/10.3389/fnhum.2013.00937>
- Wang, B., Zhan, Q., Yan, T., Imtiaz, S., Xiang, J., Niu, Y., Liu, M., Wang, G., Cao, R., & Li, D. (2019). Hemisphere and gender differences in the rich-club organization of structural networks. *Cerebral Cortex*, 29(11), 4889–4901. <https://doi.org/10.1093/cercor/bhz027>
- Wang, Y., Deng, F., Jia, Y., Wang, J., Zhong, S., Huang, H., Chen, L., Chen, G., Hu, H., Huang, L., & Huang, R. (2019). Disrupted rich club organization and structural brain connectome in unmedicated bipolar disorder. *Psychological Medicine*, 49(3), 510–518. <https://doi.org/10.1017/S0033291718001150>
- Watanabe, T. (2013). Rich-club network topology to minimize synchronization cost due to phase difference among frequency-synchronized oscillators. *Physica A: Statistical Mechanics and its Applications*, 392(5), 1246–1255. <https://doi.org/10.1016/j.physa.2012.11.041>
- Welton, T., Kent, D. A., Auer, D. P., & Dineen, R. A. (2015). Reproducibility of graph-theoretic brain network metrics: A systematic review. *Brain Connectivity*, 5(4), 193–202. <https://doi.org/10.1089/brain.2014.0313>
- Williams, G., Palminteri, S., & Haggard, P. (2022, February 1). Assembling hierarchies of action using sequencing and abstraction: Studies and models of zero-shot learning assembling hierarchies of action using sequencing and abstraction: Studies and models of zero-shot learning. <https://doi.org/10.31234/osf.io/gzjur>
- Wolff, A., Berberian, N., Golesorkhi, M., Gomez-Pilar, J., Zilio, F., & Northoff, G. (2022). Intrinsic neural timescales: Temporal integration and segregation. *Trends in Cognitive Sciences*, 26(2), 159–173. <https://doi.org/10.1016/j.tics.2021.11.007>
- Wong, B., & Szűcs, D. (2013). Single-digit Arabic numbers do not automatically activate magnitude representations in adults or in children: Evidence from the symbolic same-different task. *Acta Psychologica*, 144(3), 488–498. <https://doi.org/10.1016/j.actpsy.2013.08.006>

- Wu, K., Taki, Y., Sato, K., Sassa, Y., Inoue, K., Goto, R., Okada, K., Kawashima, R., He, Y., Evans, A. C., & Fukuda, H. (2011). The overlapping community structure of structural brain network in young healthy individuals. *PLoS One*, 6(5), 1–14. <https://doi.org/10.1371/journal.pone.0019608>
- Yan, T., Wang, W., Yang, L., Chen, K., Chen, R., & Han, Y. (2018). Rich club disturbances of the human connectome from subjective cognitive decline to Alzheimer's disease. *Theranostics*, 8(12), 3237–3255. <https://doi.org/10.7150/thno.23772>
- Yedetore, A., Linzen, T., Frank, R., & McCoy, R. T. (2023). How poor is the stimulus? Evaluating hierarchical generalization in neural networks trained on child-directed speech. Retrieved from <http://arxiv.org/abs/2301.11462>
- Yeh, C.-H., Smith, R. E., Liang, X., Calamante, F., & Connelly, A. (2018). Investigating the streamline count required for reproducible structural connectome construction across a range of brain parcellation resolutions. *Proceedings of ISMRM*, 1558, 1–4. <http://cds.ismrm.org/protected/18MPresentations/abstracts/1558.html>
- Yeh, F. C., Wedeen, V. J., & Tseng, W. Y. I. (2010). Generalized q-sampling imaging. *IEEE Transactions on Medical Imaging*, 29(9), 1626–1635. <https://doi.org/10.1109/TMI.2010.2045126>
- Zamora-López, G., Zhou, C., & Kurths, J. (2010). Cortical hubs form a module for multisensory integration on top of the hierarchy of cortical networks. *Frontiers in Neuroinformatics*, 4(MAR), 1–13. <https://doi.org/10.3389/neuro.11.001.2010>

SUPPORTING INFORMATION

Additional supporting information can be found online in the Supporting Information section at the end of this article.

How to cite this article: Mecklenbrauck, F., Gruber, M., Siestrup, S., Zahedi, A., Grotegerd, D., Mauritz, M., Trempler, I., Dannlowski, U., & Schubotz, R. I. (2023). The significance of structural rich club hubs for the processing of hierarchical stimuli. *Human Brain Mapping*, 1–28. <https://doi.org/10.1002/hbm.26543>